MODELLING AND SIMULATION OF METAL CUTTING BY FINITE ELEMENT METHOD

A Thesis Submitted to
the Graduate School of Engineering and Sciences of
İzmir Institute of Technology
in Partial Fulfilment of the Requirements for the Degree of

MASTER OF SCIENCE

in Mechanical Engineering

by
CENK KILIÇASLAN

December 2009
İZMİR

We approve the thesis of **Cenk KILIÇASLAN**

Assoc. Prof. Dr. Bülent YARDIMOĞLU
Supervisor

Prof. Dr. Ramazan KARAKUZU
Committee Member

Assist. Prof. Dr. H. Seçil ARTEM
Committee Member

18 December 2009

Prof. Dr. Metin TANOĞLU
Head of the Department of
Mechanical Engineering

Assoc. Prof. Dr. Talat YALÇIN
Dean of the Graduate School of
Engineering and Sciences

ACKNOWLEDGEMENTS

I would like to thank my advisor, Bülent Yardımoğlu, for his kindness, help and patience during my research. Lastly my greatest regards go to my family and colleagues in my office for their support and encouragement during the period of my graduate education.

ABSTRACT

MODELLING AND SIMULATION OF METAL CUTTING BY FINITE ELEMENT METHOD

Metal cutting is one of the most widely used manufacturing techniques in the industry and there are lots of studies to investigate this complex process in both academic and industrial world. Predictions of important process variables such as temperature, cutting forces and stress distributions play significant role on designing tool geometries and optimising cutting conditions. Researchers find these variables by using experimental techniques which makes the investigation very time consuming and expensive. At this point, finite element modelling and simulation becomes main tool. These important cutting variables can be predicted without doing any experiment with finite element method.

This thesis covers a study on modelling and simulation of orthogonal metal cutting by finite element method.

For this purpose, orthogonal cutting simulations of AISI 1045 steel are performed and model used in simulations is validated. At first step, effects of work piece flow stress and friction models on cutting variables such as cutting forces, chip geometry and temperature are investigated by comparing simulation results with experimental results available in the literature. Then, mechanical and thermal analyses are performed. Lastly, effects of rake angle and tool tip radius on strain, temperature and stress distributions are investigated.

ÖZET

SONLU ELEMANLAR METODU İLE METAL KESMENİN MODELLENMESİ VE BENZETİMİ

Metal kesme endüstride en çok kullanılan imalat tekniklerinden biridir ve hem akademik hem de endüstri dünyasında bu karmaşık işlemi inceleyen birçok çalışma vardır. Sıcaklık, kesme kuvvetleri ve gerilme dağılımları gibi önemli işlem değişkenlerinin tahmini, takım geometrilerinin tasarımında ve kesme koşullarının eniyilenmesinde önemli bir rol oynar. Araştırmacılar bu değişkenleri, araştırmayı çok zaman alıcı ve pahalı hale getiren deneysel teknikler kullanarak bulurlar. Bu noktada sonlu elemanlar modellemesi ve benzetimi ana araç haline gelir. Bu önemli kesme değişkenleri herhangi bir deneye gerek kalmadan sonlu elemanlar metodu ile tahmin edilebilirler.

Bu tez, dik metal kesmenin sonlu elemanlar metodu ile modellenmesi ve benzetimi çalışmasını içermektedir.

Bu amaçla, AISI 1045 çeliğinin dik kesme benzetimleri gerçekleştirilmiş ve benzetimlerde kullanılan model doğrulanmıştır. İlk adımda, iş parçası akış gerilmesi ve sürtünme modellerinin, kesme kuvvetleri, talaş geometrisi ve sıcaklık gibi kesme değişkenlerine olan etkileri, benzetim sonuçlarının ve literatürde mevcut deneysel sonuçların karşılaştırılması ile incelenmiştir. Daha sonra, mekanik ve ısıl analizler gerçekleştirilmiştir. Son olarak, talaş açısı ve takım ucu radyusunun, birim şekil değiştirme, sıcaklık ve gerilme dağılımlarına olan etkileri incelenmiştir.

TABLE OF CONTENTS

LIST OF FIGURES viii

LIST OF TABLES xi

LIST OF SYMBOLS xii

CHAPTER.1. INTRODUCTION 1

CHAPTER.2. MECHANICS OF ORTHOGONAL METAL CUTTING 3

2.1. Introduction 3

2.2. Mechanics of Orthogonal Metal Cutting 5

2.2.1. Thin Zone Model 6

2.2.2. Thick Zone Model 13

2.3. Friction in Metal Cutting 18

2.4. Shear Stress in Metal Cutting 20

2.5. Temperature in Metal Cutting 20

CHAPTER.3. FINITE ELEMENT SIMULATION OF METAL CUTTING 22

3.1. Introduction 22

3.2. Model Formulation 22

3.2.1. Lagrangian 22

3.2.2. Eulerian 23

3.2.3. Arbitrary Lagrangian-Eulerian 23

3.3. Meshing 24

3.4. Work Material Constitutive Models 25

3.4.1. Oxley Material Model 26

3.4.2. Johnson and Cook Material Model 26

3.4.3. Zerilli and Armstrong Material Model 27

3.5. Friction Models 27

3.5.1. Constant Coulomb 28

3.5.2. Constant Shear 28

3.5.3. Constant Shear in Sticking Zone and Coulomb in Sliding Zone 28
3.6. Chip Separation Criteria 29
3.7. FE Software Packages and Utilization..... 30

CHAPTER.4. PRESENT MODEL AND SIMULATION OF METAL CUTTING..... 33
4.1. Introduction..... 33
4.2. Tool Modelling 33
4.3. Work piece Modelling 34
4.4. System Modelling..... 42

CHAPTER.5. RESULTS AND DISCUSSION..... 46
5.1. Introduction..... 46
5.2. Comparison of Material Constitutive Models 46
5.3. Comparison of Friction Models 48
5.4. Analysis of Mechanical and Thermal Parameters 52
5.5. Effects of Rake Angles 54
5.6. Effects of Tool Tip Radii 62

CHAPTER.6. CONCLUSION 68

REFERENCES 70

LIST OF FIGURES

Figure **Page**

Figure 2.1. Types of cutting: (a) Orthogonal cutting, (b) Oblique cutting 3
Figure 2.2. Chip samples: (a) Discontinuous, (b) Continuous, (c) Continuous with Built-up edge 4
Figure 2.3. Variables in orthogonal cutting 4
Figure 2.4. Deformation zones in metal cutting 5
Figure 2.5. Merchant's orthogonal force diagram 6
Figure 2.6. Relation between shear angle: (a) Chip thickness, (b) Velocities 8
Figure 2.7. Oxley's thin shear model 10
Figure 2.8. Mohr stress circle at point B 11
Figure 2.9. Stress distribution on the rake face 12
Figure 2.10. Deformation model for thick-zone 14
Figure 2.11. Palmer and Oxley's contact suggestion 16
Figure 2.12. Geometry of Palmer and Oxley cutting analysis 17
Figure 2.13. Distribution of shear and normal stress on the rake face 19
Figure 2.14. Pre-flow region 20
Figure 2.15. Locations of heat sources in metal cutting 21
Figure 3.1. Eulerian and Lagrangian boundary conditions in ALE simulation 24
Figure 3.2. Refinement: (a) Initial local mesh, (b) Reducing element size 25
Figure 3.3. Smoothing: (a) Initial local mesh, (b) Reallocating of the nodes 25
Figure 3.4. Geometrical Separation 29
Figure 3.5. Orthogonal metal cutting simulation by using Abaqus 31
Figure 3.6. Modelling by using Advantedge; (a) 2D Turning, (b) 3D Turning, (c) Drilling, (d) Cylindrical Milling 32
Figure 3.7. Metal cutting simulation by using Ls-Dyna 32
Figure 4.1. Mesh design of the tool 34
Figure 4.2. AISI 1045 Oxley flow curve at T=20 ºC 35
Figure 4.3. AISI 1045 Oxley flow curve at T=300 ºC 36
Figure 4.4. AISI 1045 Oxley flow curve at T=900 ºC 36
Figure 4.5. AISI 1045 Johnson-Cook flow curve at T=20 ºC 37
Figure 4.6. AISI 1045 Johnson-Cook flow curve at T=300 ºC 37

Figure 4.7. AISI 1045 Johnson-Cook flow curve at T=900 ºC 38
Figure 4.8. AISI 1045 Zerilli-Armstrong flow curve at T=20 ºC 38
Figure 4.9. AISI 1045 Zerilli-Armstrong flow curve at T=300 ºC 39
Figure 4.10. AISI 1045 Zerilli-Armstrong flow curve at T=900 ºC 39
Figure 4.11. Mesh design of the work piece 40
Figure 4.12. Thermal Conductivity of AISI 1045 41
Figure 4.13. Thermal Expansion of AISI 1045 41
Figure 4.14. Heat capacity of AISI 1045 42
Figure 4.15. Displacement boundary conditions of the cutting system 43
Figure 4.16. Thermal boundary conditions of the cutting system 44
Figure 4.17. Contact generation between the tool and the work piece 44
Figure 4.18. Remeshing procedure at cutting zone; (a) Initial mesh distribution, (b) Mesh distortion, (c) New mesh generation 45
Figure 5.1. Temperature distribution 52
Figure 5.2. Plastic strain distribution 53
Figure 5.3. Strain rate distribution 53
Figure 5.4. Effective stress distribution 54
Figure 5.5. Strain distribution for α = -10º 55
Figure 5.6. Strain distribution for α = 0º 55
Figure 5.7. Strain distribution for α = 10º 56
Figure 5.8. Temperature distribution for α = -10º 56
Figure 5.9. Temperature distribution for α = 0º 57
Figure 5.10. Temperature distribution for α = 10º 57
Figure 5.11. Effective stress distribution for α = -10º 58
Figure 5.12. Effective stress distribution for α = 0º 58
Figure 5.13. Effective stress distribution for α = 10º 59
Figure 5.14. The steady state tool temperature for α = -10º 60
Figure 5.15. The steady state tool temperature for α = 0º 60
Figure 5.16. The steady state tool temperature for α = 10º 61
Figure 5.17. Stress distribution in the tool for α = -10º 61
Figure 5.18. Stress distribution in the tool for α = 0º 62
Figure 5.19. Stress distribution in the tool for α = 10º 62
Figure 5.20. Strain distribution in the chip and the work piece for r_T = 5 µm 63
Figure 5.21. Strain distribution in the chip and the work piece for r_T = 50 µm 63

Figure 5.22. Strain distribution in the chip and the work piece for r_T = 68 μm 64
Figure 5.23. Temperature distribution in the tool for r_T = 5 μm.....64
Figure 5.24. Temperature distribution in the tool for r_T = 50 μm.....65
Figure 5.25. Temperature distribution in the tool for r_T = 68 μm.....65
Figure 5.26. Stress distribution in the tool for r_T = 5 μm 66
Figure 5.27. Stress distribution in the tool for r_T = 50 μm 66
Figure 5.28. Stress distribution in the tool for r_T = 68 μm 67

LIST OF TABLES

Table **Page**

Table 4.1. Geometric variables of the cutting tool 33
Table 4.2. Thermal and mechanical properties of WC 33
Table 4.3. Constants for Johnson-Cook constitutive model 35
Table 4.4. Constants for Zerilli-Armstrong constitutive model 35
Table 4.5. Cutting conditions 42
Table 5.1. Experimental results 46
Table 5.2. Cutting force and thrust force results for different material models 47
Table 5.3. Chip geometry results for different material models 47
Table 5.4. Temperature results for different material models 48
Table 5.5. Effect of shear friction factors on the chip geometry 48
Table 5.6. Effect of shear friction factors on cutting and thrust force 49
Table 5.7. Effect of shear friction factors on temperature 49
Table 5.8. Effect of Coulomb friction coefficients on the chip geometry 49
Table 5.9. Effect of Coulomb friction coefficients on cutting and thrust force 50
Table 5.10. Effect of Coulomb friction coefficients on temperature 50
Table 5.11. Constant shear friction in sticking zone and Coulomb friction model in sliding zone (Hybrid Model) 50
Table 5.12. Effect of hybrid friction model on chip geometry 51
Table 5.13. Effect of hybrid friction model on cutting and thrust force 51
Table 5.14. Effect of hybrid friction model on temperature 51

LIST OF SYMBOLS

A	Yield stress
b	Width of cut
B	Hardening modulus
c	Clearance angle
C	Strain rate sensitivity
dS	Elemental length of slip line
F	Friction force on the rake face
F_N	Normal force
F_P	Power force
F_Q	Thrust Force
F_R	Radial force
F_S	Shear force
h	Tool-chip contact length
h_{int}	Interface heat transfer coefficient
i	Cutting edge inclination
k	Material shear flow stress
l	Length of the cut
L_c	Contact length between the chip and the tool
l_{chip}	Length of the chip
m	Thermal softening coefficient
N	Normal force on the rake face
n	Strain hardening coefficient
ø	Shear angle
P	Hydrostatic Stress
R	Resultant force
r	Chip thickness ratio
r_T	Tool tip radius
t	Undeformed chip thickness
t_c	Chip thickness
T	Instantaneous temperature
T_m	Melting temperature

T_{mod}	Velocity modified temperature
T_r	Room temperature
V_c	Chip velocity
V_s	Shear velocity
V_w	Cutting velocity
α	Rake angle
β	Friction angle
$\dot{\gamma}$	Shear strain rate
γ	Shear strain
Δy	Thickness of shear zone
$\dot{\varepsilon}$	Strain rate
$\dot{\varepsilon}_0$	Reference strain rate
ε	Strain
σ	Normal stress
τ	Shear stress

CHAPTER 1

INTRODUCTION

Machining is one of the most widely used production technique in industry for converting preformed blocks of metal into desired shapes with surface quality and dimensional accuracy. These shaping operations are done in forms of metal chips.

Metal cutting studies are as old as over 100 years. Early research in metal cutting started with Cocquilhat (1851), who was focused on the work required to remove a given volume of material in drilling. Tresca (1873) firstly attempted to explain how chips are formed. Ernest and Merchant (1941) first developed the simplest and most widely used model for cutting. Lee and Shaffer (1951), Kobayashi and Thomsen (1962) contributed to study of Ernest and Merchant. Oxley and Welsh (1963) introduced the first parallel-sided shear zone model of chip formation for a predictive machining theory. Most widely used text books are written by Armerago (1969), Boothroyd (1981), Shaw (1984) and Trent (2000). More general introductory knowledge can be found at text books written by Kalpakjian, et al. (2006), and DeGarmo, et al. (1997).

The experimental approach to study machining process is expensive and time consuming especially when a wide range of parameters included like tool geometry, materials, cutting conditions and so on. Because of these difficulties alternative approaches developed as mathematical simulations where numerical methods are used. Among these numerical methods, finite element method is proved to be useful and widely used.

Finite element method is basically defined as dividing a continuum system to small elements, describes element properties as matrices and assembles them to reach a system of equations whose solutions give the behaviour of the total system.

Basic ideas of the finite element method are studied at the beginning of 1940s. Courant (1943) developed finite element method and he used piecewise polynomial interpolation over triangular subregions to model torsion problems. Clough (1960) used the term “finite element” firstly. Zienkiewicz and Cheung (1967) wrote the first book on finite element theory. Also other theory books are written by Cook, et al. (1989), Mohr (1992) and Chandrupatla and Belegundu (2002).

Finite element method has a great use in modelling orthogonal (2D) and oblique (3D) metal cutting. Klamecki (1973) developed one of the first finite element models for metal cutting processes by using an updated Lagrangian elasto-plastic three dimensional model which was limited to the initial stages of chip formation. Usui and Shirakashi (1982) developed the first two dimensional FE orthogonal machining simulation by using a special method of computation called the iterative convergence method to obtain solutions for steady state cutting. Iwata, et al. (1984) developed a method of numerical modelling for plane strain orthogonal cutting in the steady state on the basis of the rigid-plastic material model where temperature effects were neglected. Strenkowski and Carroll (1985) developed a numerical model for orthogonal cutting without a preformed chip. Their model was based on a large deformation updated Lagrangian code. Komvopoulos and Erpenbeck (1991) introduced a chip separation criterion using the argument of distance tolerance criterion to investigate chip formation. Lin and Lin (1992) introduced a chip separation criterion using the argument of strain energy, and investigated the chip geometry, the residual stresses in the machined surface, the temperature distributions in the chip, the tool and cutting forces. Ceretti (1996) developed a cutting model by deleting elements having reached a critical value of accumulated damage. With the developments of hardware and commercial FE codes, modelling limitations and computational difficulties have been overcome to some extent, so many researchers focused on special topics of metal cutting. Bil, et al. (2004) compared three commercial FE codes used in 2D metal cutting simulations, Msc Marc, Thirdwave Advantedge and Deform 2D, by comparing experimental results with simulation results. Özel (2006) and Filice, et al. (2007) used Deform 2D to investigate the effects of different friction models on cutting results. Attanasio, et al. (2008) included an advanced approach to model heat transfer phenomena at the tool-chip interface in the numerical simulation to investigate tool wear by using Deform 3D. Davim and Maranhao (2009) used Msc Marc to investigate plastic strain and plastic strain rate effects during high speed machining (HSM).

In this study modelling and simulation of orthogonal metal cutting is performed by using finite element method. In chapter two, theories of metal cutting are briefly discussed and historically imported analytical models are reviewed. Fundamentals of finite element modelling of metal cutting are presented in chapter three. In chapter four, present model in this study is explained. Simulation results and discussions are given in chapter five. Conclusion of the study is presented in chapter six.

CHAPTER 2

MECHANICS OF ORTHOGONAL METAL CUTTING

2.1. Introduction

Two types of cutting are used in analysis of metal cutting mechanics: Orthogonal and oblique cutting. In orthogonal cutting, unwanted material is removed from the work piece by a cutting edge that is perpendicular to the direction of relative motion between tool and the work piece as shown in Figure 2.1.

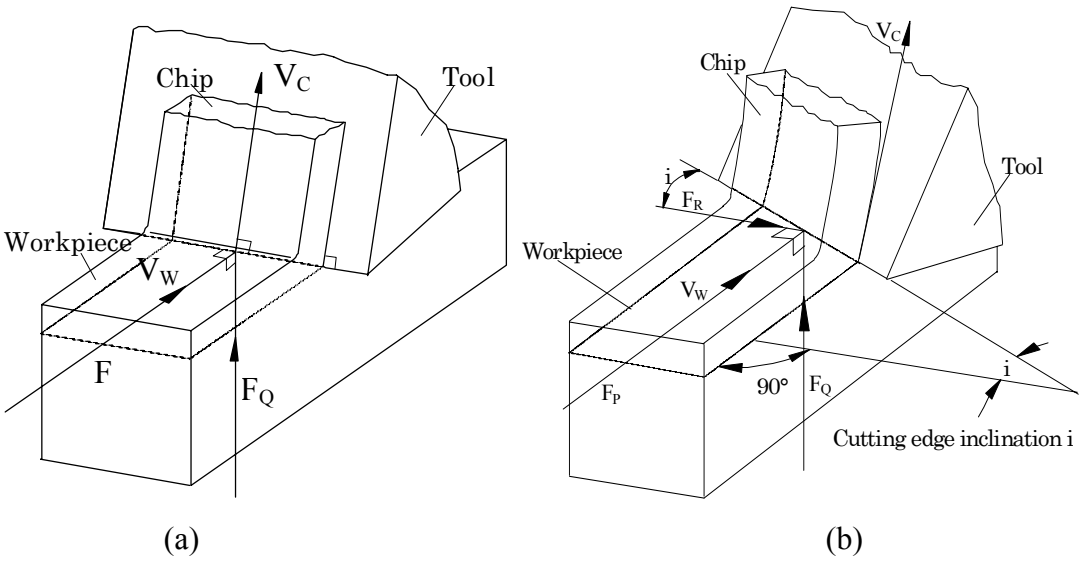

Figure 2.1. Types of cutting: (a) Orthogonal cutting, (b) Oblique cutting

In orthogonal cutting, the material removal process is assumed to be uniform along the cutting edge; therefore it is a two dimensional plane strain problem. In oblique cutting, the major cutting edge is inclined to direction of the cutting velocity with an inclination angle as shown in Figure 2.1.

Although most of the metal cutting operations are oblique, orthogonal cutting has been extensively studied because of its simplicity and giving good approximations.

The chip formation of oblique and orthogonal cutting is approximately identical. In machining operations, there are three types of chips occur: Discontinuous chips, continuous chips and continuous chip with built-up edge (BUE).

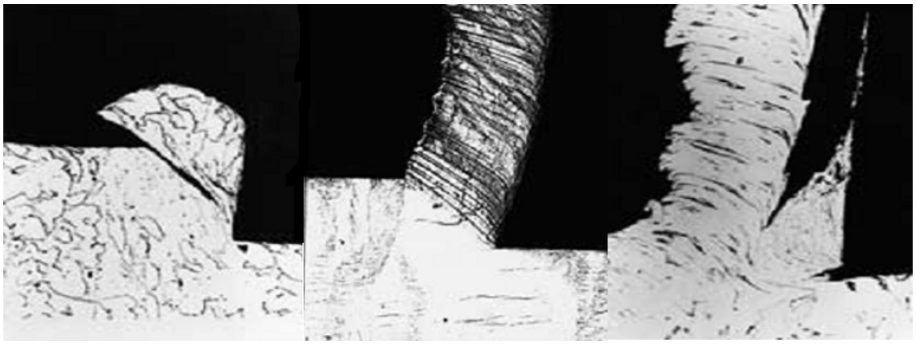

(a) (b) (c)

Figure 2.2. Chip samples: (a) Discontinuous, (b) Continuous, (c) Continuous with build up edge. (Source: Childs, et al. 2000)

Discontinuous chip occurs when brittle metals are cut such as cast iron or when some ductile metals are machined under low cutting speeds. Machine vibration or tool chatter may cause this type of chips form. Continuous chip is produced when ductile metals are cut or cutting with high speeds. This type of chip is considered ideal for cutting operation because it results in better surface finish. Continuous chip with built-up edge forms when low carbon machining steels are cut with high speed steel cutting tools under low cutting speeds. BUE results poor surface finish and it shortens tool life. High cutting speeds can be used to eliminate BUE.

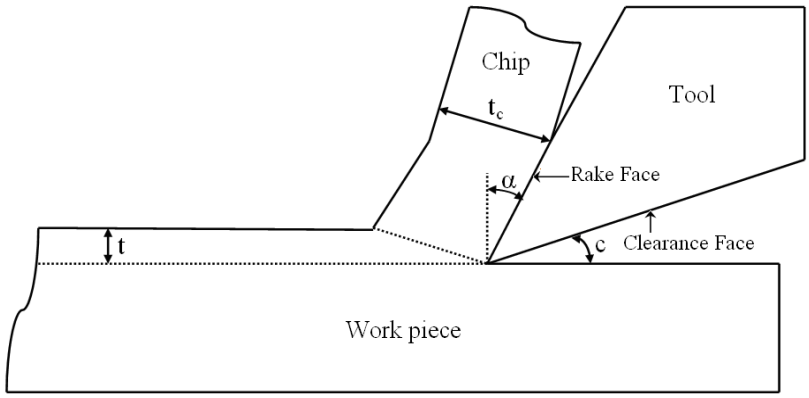

Figure 2.3. Variables in orthogonal cutting

Orthogonal cutting and tool geometry variables are shown in Figure 2.3. t is the undeformed chip thickness and it is sometimes called depth of cut. t_c is the chip thickness. Rake face is the face where chip and tool in contact. Rake angle (α) is an angle between the rake face and newly machined surface normal. Clearance face is a surface which the machined surface passes over. Clearance angle (c) is an angle between newly machined surface and clearance face. These variables are important because they determine the characteristics of the process.

There are three deformation zones in the cutting process as shown in Figure 2.4.;

- Primary shear zone (A-B): The chip formation takes place firstly and mainly in this zone as the edge of the tool penetrates into the work-piece. Material on this zone has been deformed by a concentrated shearing process.
- Secondary shear zone (A-C): The chip and the rake face of the tool are in contact from A to C. When the frictional stress on the rake face reaches a value equal to the shear yield stress of the work-piece material, material flow also occur on this zone.
- Tertiary shear zone (A-D): When the clearance face of the tool rubs the newly machined surface deformation can occur on this zone.

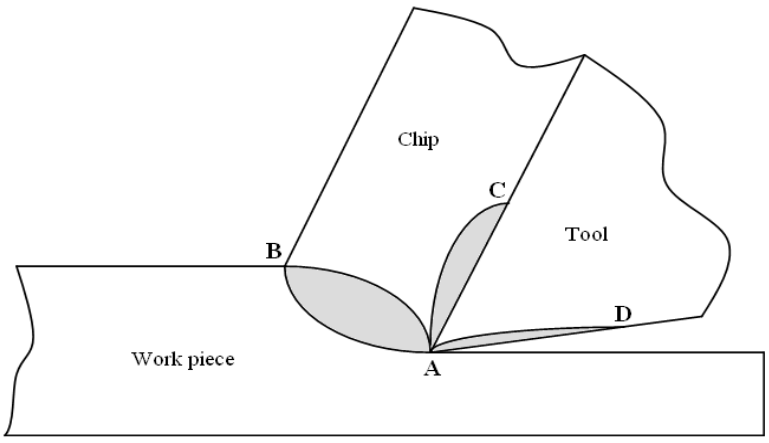

Figure 2.4. Deformation zones in metal cutting

2.2. Mechanics of Metal Cutting

In the last sixty years researchers have been focused on predicting physical behaviour of metal cutting or developing previous models. Much of the early works are

analytical models that represent the basic mechanics of metal cutting. Two basic models of thought in the approach to the analysis; thin zone which describe the cutting process at high cutting speeds and thick zone model which describe the cutting process at low cutting speeds.

2.2.1. Thin Zone Model

Merchant (1945) developed an analysis for thin-zone model with the following assumptions:

i) Tool tip is sharp, and no rubbing occurs between the tool and the work piece.

ii) The deformation is two dimensional.

iii) The stresses on the shear plane are uniformly distributed.

iv) The resultant force R applied at the shear plane is equal, opposite and collinear to the force R applied to the chip at the tool-chip interface.

With the help of these assumptions, force diagram of orthogonal cutting can be drawn as shown in Figure 2.5.

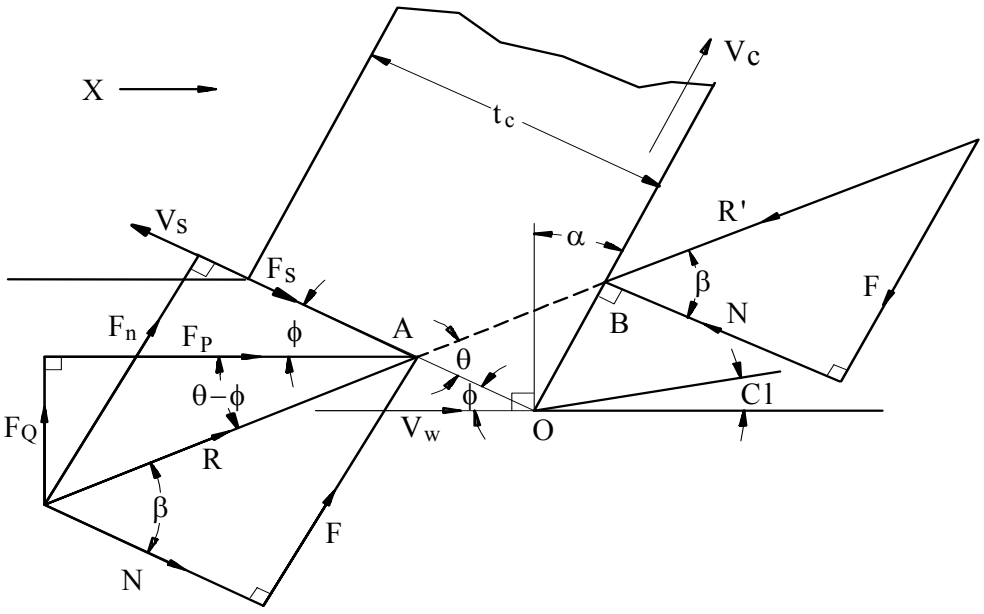

Figure 2.5. Merchant's orthogonal force diagram

The resultant force can be related to the other forces such as friction force F along the rake face or the power force F_P in the direction of motion. Since the resultant force can change in magnitude and direction, it is better to consider the two force components F_P (along the work velocity) and F_Q (perpendicular to work velocity). These forces are given as

$$F_P = \frac{tb\tau\cos(\beta-\alpha)}{\sin\phi\cos(\phi+\beta-\alpha)} \tag{2.1}$$

$$F_Q = \frac{tb\tau\sin(\beta-\alpha)}{\sin\phi\cos(\phi+\beta-\alpha)} \tag{2.2}$$

where τ is the shear stress on the shear plane assumed uniform over this plane and equal to shear yield stress of the work-piece material, Ø is the shear angle shown in Figure 2.5., α is the tool rake angle, t is the undeformed chip thickness, b is the width of cut, and β is the angle between the resultant force and the normal to the rake face. This angle represents the friction angle between the tool and chip. From the Equations 2.1 and 2.2 the cutting forces can be determined if shear stress, friction angle and shear angle are known.

Shear angle is an important variable in metal cutting analysis because it defines the characteristic of deformation. Merchant used the minimum energy principle in his analysis and he assumed that the deformation process adjusted itself to a minimum energy condition. He applied this assumption by equating $dF_P/d\text{Ø}$ to zero for a constant cutting speed;

$$\frac{dF_P}{d\phi} = \frac{tb\tau\cos(\beta-\alpha)\cos(2\phi+\beta-\alpha)}{\sin^2\phi\cos^2(\phi+\beta-\alpha)} = 0 \tag{2.3}$$

Then

$$\phi = \frac{\pi}{4} - \frac{1}{2}(\beta-\alpha) \tag{2.4}$$

This approach has two doubts. Firstly, he used minimum energy principle, which is not supported by evidence. Secondly, the differentiation assumes β and τ are constants but β is not a constant and it is dependent of shear angle.

Shear angle can be determined by using length of cut or chip thickness.

$$\frac{l_{chip}}{l} = \frac{t_c}{t} = r \tag{2.5}$$

Where l is the length of the cut, l_{chip} is the length of the chip, t is the undeformed chip thickness, t_c is the chip thickness and r is the chip ratio. By using the geometry of the cut which is shown in Figure 2.6., shear angle can be obtained by

$$\tan\phi = \frac{r\cos\alpha}{1 - r\sin\alpha} \tag{2.6}$$

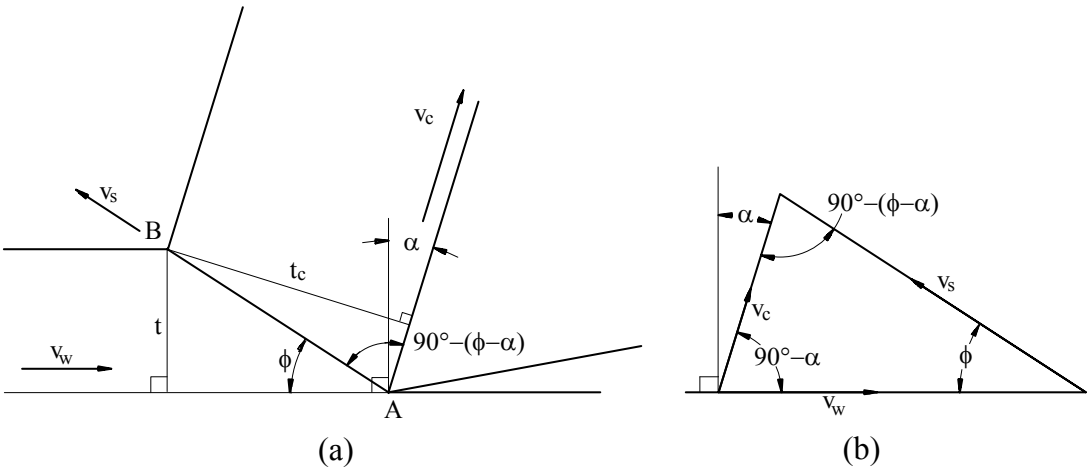

Figure 2.6. Relation between shear angle: (a) Chip thickness, (b) Velocities

From the force diagram in Figure 2.5., shear force F_S and normal force F_N are given by

$$F_S = F_P\cos\phi - F_Q\sin\phi \tag{2.7}$$

$$F_N = F_P\sin\phi + F_Q\cos\phi \tag{2.8}$$

The shear stress τ and normal stress σ can be obtained with the help of

$$\tau = \frac{F_S}{A_S} = \frac{\left(F_P \cos\phi - F_Q \sin\phi\right)\sin\phi}{bt} \tag{2.9}$$

$$\sigma = \frac{\left(F_P \sin\phi + F_Q \cos\phi\right)\sin\phi}{bt} \tag{2.10}$$

From the velocity diagram in Figure 2.7., chip velocity and shear velocity can be obtained by using:

$$V_C = \frac{\sin\phi}{\cos(\phi - \sigma)} V_w = r V_w \tag{2.11}$$

$$V_S = \frac{\cos\alpha}{\cos(\phi - \alpha)} V_w \tag{2.12}$$

Shear strain and strain rate in cutting is given by

$$\gamma = \tan(\phi - \alpha) + \cot\phi \tag{2.13}$$

$$\dot{\gamma} = \frac{V_S}{\Delta y} = \frac{\cos\alpha}{\cos(\phi - \alpha)} \frac{V_w}{\Delta y} \tag{2.14}$$

where Δy is the thickness of the shear zone.

In Merchant's analysis, the contact between the tool and the chip is Coulomb friction and the following formula for coefficient of friction can be obtained from force diagram shown in Figure 2.5.

$$\mu = \frac{F}{N} = \frac{F_P \sin\alpha + F_Q \cos\alpha}{F_P \cos\alpha - F_Q \sin\alpha} = \frac{F_Q + F_P \tan\alpha}{F_P - F_Q \tan\alpha} = \tan\beta \tag{2.15}$$

Where F is the friction force on the rake face, N is the normal force on the rake face.

Another thin shear model is derived by Oxley (1961). The model is shown in Figure 2.7. He used a simplified slip line field in his metal cutting analysis with the following assumptions:

i) There is no force at the tool tip.

ii) The tangential and normal stresses on the rake face are distributed uniformly.

iii) The distance between point A and the free surface is negligible.

iv) The deformation zone is bounded by straight and parallel slip lines at an angle ø and slip line DC meet the free surface at 45º at point O.

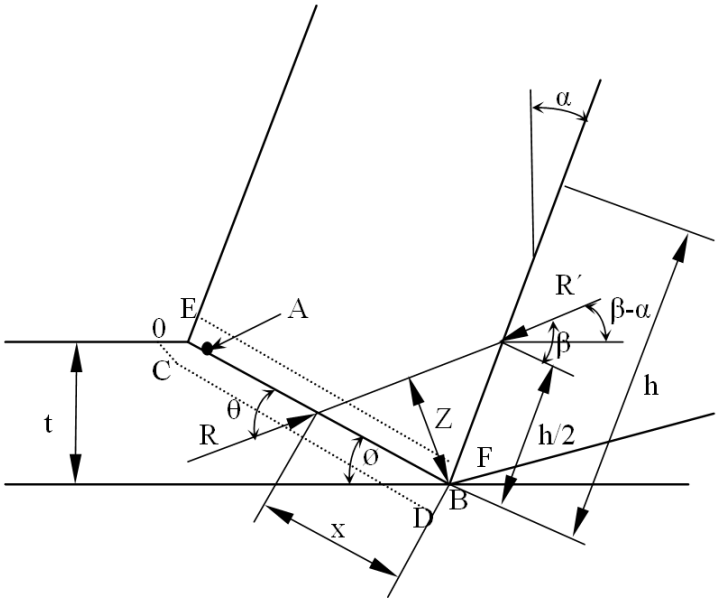

Figure 2.7. Oxley's thin shear model

Hencky relationships were used to describe the stress condition by Oxley as shown in Equation 2.16.

$$P + 2k\psi + \int \frac{\partial k}{\partial S_2} dS_1 = \text{Constant along I}$$

$$P - 2k\psi + \int \frac{\partial k}{\partial S_1} dS_2 = \text{Constant along II} \qquad (2.16)$$

Where ψ is the angle between a tangent to slip line I at any point and a reference axis.

Oxley calculated the hydrostatic stress at point A using Equation 2.16. Point A is very close to the free surface therefore the work hardening term can be neglected. It is given as

$$P_A = k\left[1 + 2\left(\frac{\pi}{4} - \phi\right)\right] \tag{2.17}$$

The hydrostatic stress at point B is given as

$$P_B = P_A - \frac{\Delta k}{\Delta S_1}\frac{t}{\sin\phi} \tag{2.18}$$

The direction of the resultant force is given by

$$\tan\theta = \frac{P_A + P_B}{2k} \tag{2.19}$$

The stresses on the slip line AB can be written in terms of the stresses on the rake face of the tool by using Mohr stress circle at point B as shown in Figure 2.8.

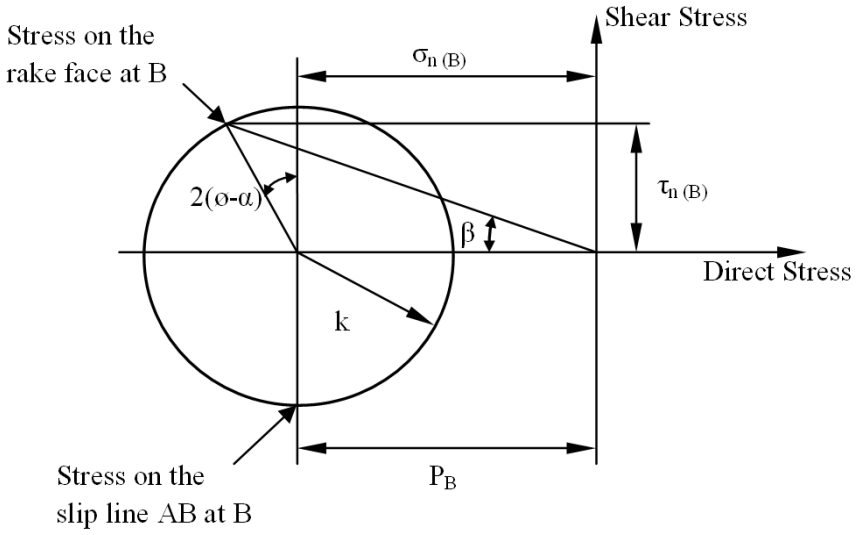

Figure 2.8. Mohr stress circle at point B

Therefore P_B can be written as

$$P_B = k\left[\frac{\cos 2(\phi-\alpha)}{\tan\beta} - \sin 2(\phi-\alpha)\right] \tag{2.20}$$

The angle θ between resulting cutting force and the shear plane can be obtained by using Equation 2.17, 2.19 and 2.20. It is given as

$$\theta = \tan^{-1}\left[\frac{1}{2} + \frac{\pi}{4} - \phi + \frac{\cos 2(\phi-\alpha)}{2\tan\beta} - \frac{\sin 2(\phi-\alpha)}{2}\right] \tag{2.21}$$

The forces R and R' are equal and opposite. The angle between R' and the cutting direction is (β-α) as shown in Figure 2.7. Therefore, the angle θ can be written as

$$\theta = \phi + \beta - \alpha \tag{2.22}$$

Oxley made several modifications to his basic assumptions. The most important one is to take account the nonuniform stress distribution on the rake face of the tool as shown in Figure 2.9.

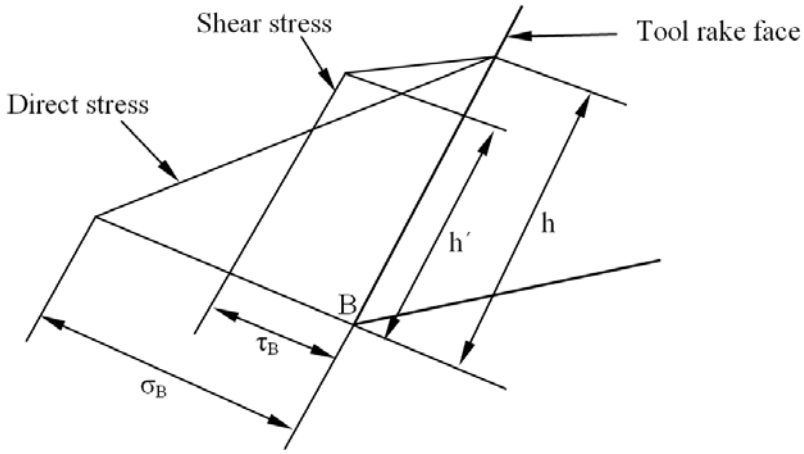

Figure 2.9. Stress distribution on the rake face

The friction angle can be defined as

$$\beta = \frac{F}{N} \tag{2.23}$$

Shear and normal stress at point B can be written as follows:

$$F = \frac{\tau_B}{2}\left(h + h^{'}\right)b \tag{2.24}$$

$$N = \frac{\sigma_B}{2}hb \tag{2.25}$$

Thus the friction angle becomes:

$$\tan\beta = \frac{\tau_B}{\sigma_B}\left(1 + \frac{h^{'}}{h}\right) \tag{2.26}$$

The Mohr circle for point B is the same. However, β in the diagram is not the average friction angle. It is called the instantaneous value at point B. It is given by

$$\tan\beta_B = \frac{\tau_B}{\sigma_B} = \frac{\tan\beta}{\left(1 + \frac{h^{'}}{h}\right)} \tag{2.27}$$

Therefore Equation 2.21 becomes:

$$\theta = \tan^{-1}\left[\frac{1}{2} + \frac{\pi}{4} - \phi + \left(1 + \frac{h^{'}}{h}\right)\frac{\cos 2(\phi - \alpha)}{2\tan\beta} - \frac{\sin 2(\phi - \alpha)}{2}\right] \tag{2.28}$$

2.2.2. Thick Zone Model

The analysis for the thick-zone model in orthogonal cutting has more complexity and requires more assumptions.

Okushima and Hitomi (1961) made the following analysis for the thick-zone model.

The work piece material assumed to be ideally plastic and the shear stresses on OA, OB, and OD are equal to the material shear-flow stress.

$$\tau_{OA} = \tau_{OB} = \tau_{OD} = k \tag{2.29}$$

Form equilibrium, one can write:

$$\tau_{OA} = \frac{R \sin \phi_1 \cos(\phi_1 - \alpha + \beta)}{bt} \tag{2.30}$$

$$\tau_{OB} = \frac{R \cos(\phi_2 - \alpha) \cos(\phi_2 - \alpha + \beta)}{bt_c} \tag{2.31}$$

$$\tau_{OD} = \frac{R \sin \beta}{bh} \tag{2.32}$$

where b is the width of cut, and h is tool-chip contact length.

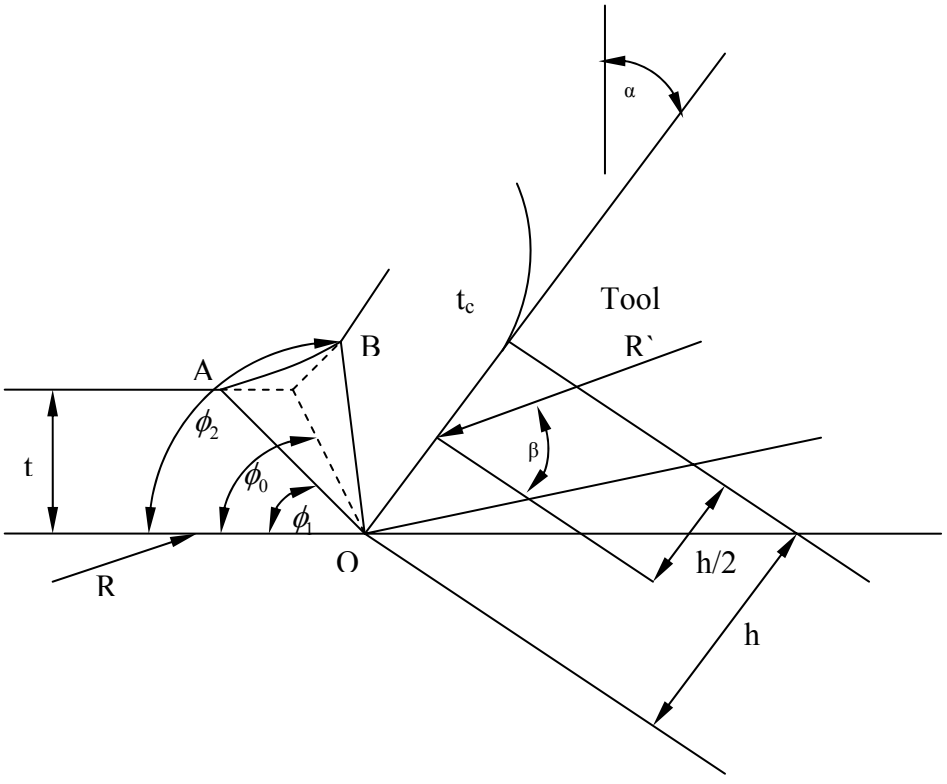

Figure 2.10. Deformation model for thick-zone

The angles φ_1 and φ_2 can be expressed as

$$\phi_1 = \frac{K_1}{2} - \frac{\beta}{2} + \frac{\alpha}{2} \tag{2.33}$$

$$\phi_2 = \frac{K_2}{2} - \frac{\beta}{2} + \frac{\alpha}{2} \tag{2.34}$$

where

$$K_1 = \sin^{-1}\left[\frac{2}{h_1}\sin\beta + \sin(\beta - \alpha)\right] \tag{2.35}$$

$$K_2 = \cos^{-1}\left[\frac{2}{h_2}\sin\beta - \cos\beta\right] \tag{2.36}$$

and

$$h_1 = \frac{h}{t} \tag{2.37}$$

$$h_2 = \frac{h}{t_c} \tag{2.38}$$

The thickness of the deformation zone Φ is represented by

$$\Phi = \phi_2 - \phi_1 = \frac{\alpha}{2} - \frac{K_1}{2} + \frac{K_2}{2} \tag{2.39}$$

Shear strains at A and B respectively for thick-zone model are:

$$\gamma_A = 0 \tag{2.40}$$

$$\gamma_B = \cot\phi_2 + \tan(\phi_2 - \alpha) \tag{2.41}$$

Another well known thick zone model was made by Palmer and Oxley (1959). They studied metal cutting at low cutting speeds and they derived slip line fields by using modified Hencky relationships. Following assumptions are made in their analysis;

i) The Hencky relationships do no consider stress discontinuity or singularity at the tool tip. They assumed that the chip and tool were not in contact at the tool tip to overcome this problem as shown in Figure 2.11.

ii) Work hardening was taken into account.

iii) The slip line AB met the free surface at 45º at point A' as shown in Figure 2.13.

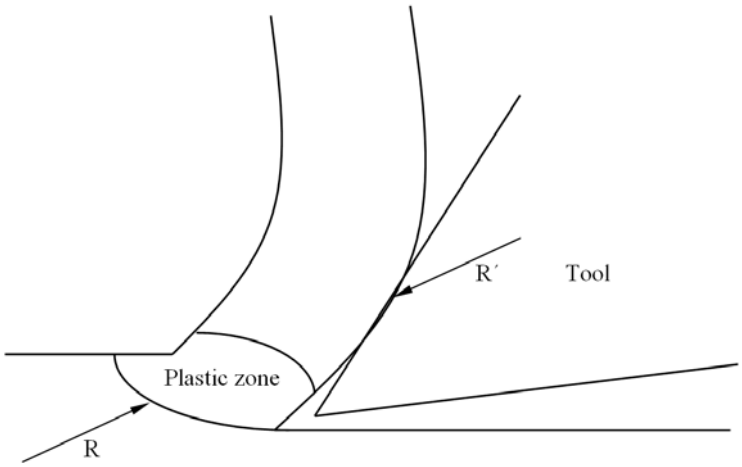

Figure 2.11. Palmer and Oxley's contact suggestion

The hydrostatic stress at point A can be written using Equation 2.16:

$$P_A = k_1\left[1 + 2\left(\frac{\pi}{4} - \phi\right)\right] = Ck_1 \tag{2.42}$$

The work hardening term in Equation 2.16 can be estimated by considering the adjacent slip line δø apart. Thus

$$\frac{\partial k}{\partial S_1} = \frac{k_2 - k_1}{\delta\phi r} = \frac{k_2 - k_1}{\delta\phi k_1}\frac{k_1}{r} = D\frac{k_1}{r} \tag{2.43}$$

k_2 is equal to the constant flow shear stress along the adjacent slip line.

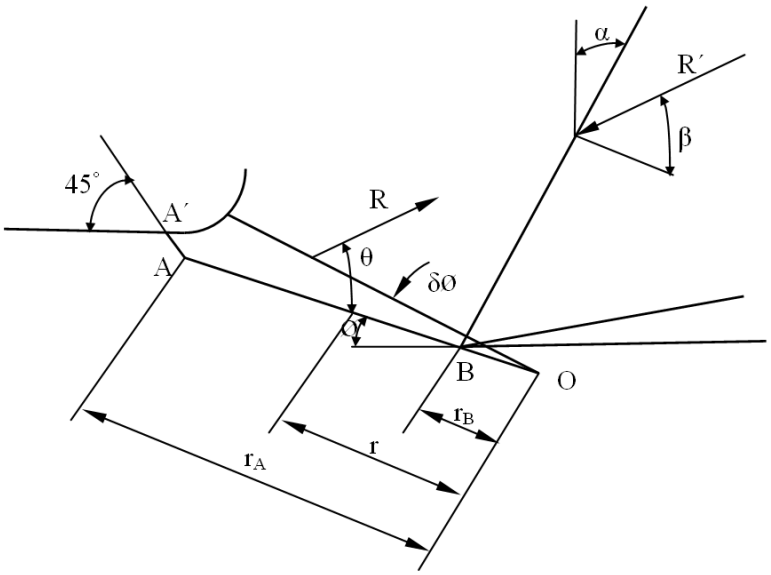

Figure 2.12. Geometry of Palmer and Oxley cutting analysis

The hydrostatic stress on AB at r can be given as

$$P_r = k_1\left[1+2\left(\frac{\pi}{4}-\phi\right)\right] - Dk_1\log_e\frac{r_A}{r} \tag{2.44}$$

The hydrostatic stress at point B is

$$P_B = k_1\left[1+2\left(\frac{\pi}{4}-\phi\right)\right] - Dk_1\log_e\frac{r_A}{r_B} \tag{2.45}$$

The normal and shear force on AB can be written as

$$F_N = k_1 b\left\{\left(r_A - r_B\right)\left[1+2\left(\frac{\pi}{4}-\phi\right)\right] - D\left[\left(r_A - r_B\right) - r_B\log\frac{r_A}{r_B}\right]\right\} \tag{2.46}$$

$$F_S = k_1 b\left(r_A - r_B\right) \tag{2.47}$$

Then

$$\tan\theta = \frac{F_N}{F_S} = \left[1 + 2\left(\frac{\pi}{4} - \phi\right) - D\left(1 - \frac{r_B}{r_A - r_B}\log_e \frac{r_A}{r_B}\right)\right] \tag{2.48}$$

The angle θ can be determined from the equilibrium of the forces on the chip and tool.

$$\theta = \phi + \beta - \alpha \tag{2.49}$$

Palmer and Oxley derived an approximate relationship between D, β and ø and they found that:

$$D \cong \cot\phi - \tan\theta \tag{2.50}$$

This analysis was criticized by many investigators because of unrealistic assumptions such as no contact between the tool tip and chip. Another weak point of this analysis is that the deformation can not be predicted analytically.

2.3. Friction in Metal Cutting

In metal cutting friction between chip and tool interface plays significant role on important process variables such as temperatures and tool wear. Therefore, it has to be studied in detail. Laws of friction was firstly determined by Leonardo da Vinci and later restated by Amonton and Coulomb. These laws are

- The friction force is proportional to the normal force which means that the coefficient of friction is constant.
- The friction force and the coefficient of friction are independent of the apparent area of the sliding interface.

These laws are valid when normal force N is below a critical certain value. In metal cutting, friction conditions are very different from a simple dry friction and normal force is very high. As the normal force increases, Coulombs' and Amontons' law no longer holds true as the real area of contact between chip and tool rake face increases. Therefore Coulomb's and Amontons' law can not represent the friction phenomenon in metal cutting.

Friction in metal cutting was studied in detail by many researchers. To achieve this goal, researchers study the contact and friction stress on the rake face by using direct measurement. Usui and Takeyama (1960) measured the distribution of the shear (τ) and the normal (σ) stress on the rake face of the tool. As shown in Figure 2.13., they found the shear stress remains constant over about the half of tool-chip contact nearest the cutting edge but it decreases to zero over the rest, reaching zero of course at point C where the chip leaves contact with the tool. The normal stress was found to decrease and reach zero from the cutting edge to point C. Zorev (1963) found also similar results from his experiments.

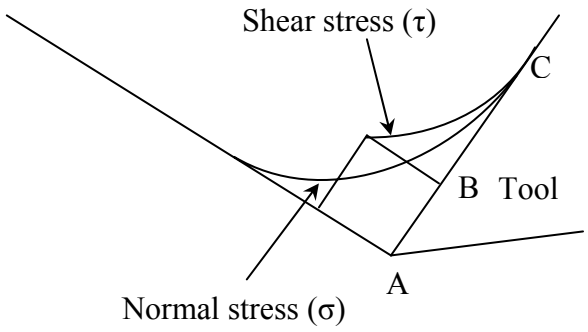

Figure 2.13. Distribution of shear and normal stress on the rake face

Over the length AB, normal stress is sufficiently high and contact area to total area ratio approaches unity and metal adheres to the rake face. This region is called the sticking region and plastic deformation occurs in the chip. The coefficient of friction in the sticking region is not constant, but it depends on the magnitude of the normal load. The value of the coefficient of friction in this region is lower than the value under sliding friction conditions. In the length from B to C, which extends from the end of the sticking region to the point where chip loses contact with the tool rake face, the contact area to total area ratio is less than unity, so coefficient of friction is constant, and sliding friction occurs.

The measured coefficient of friction in metal cutting is an average value based on both regions. Any changes in cutting conditions that may change lengths AB and BC will change the value of coefficient of friction.

2.4. Shear Stress in Metal Cutting

The shear stress in metal cutting is higher than the yield stress of determined from tensile test on work materials. Rubbing effect and the pre-flow region existence are two reasons of this situation. Rubbing effect on the clearance of the tool introduces a force which is measured but does not contribute to the shearing process. Secondly, a pre-flow region is present in most of the cutting processes that extends the length of the shear plane that assumed in analysis as shown in Figure 2.14.

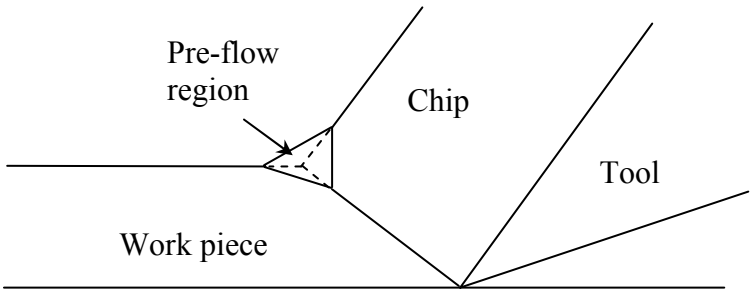

Figure 2.14. Pre-flow region

In addition to these two reasons, high normal stress can increase the yield shear stress on the shear plane during cutting. At low cutting speeds, work hardening of the material is also must be taken into account while determining the shear stress. Strain rate and temperature are normally causing opposing effects on yield stress of the material. Since both strain rate and temperature are relatively high in metal cutting operations, sometimes it can be thought as they cancel each other but recent considerations of the mechanism of yield at very high strain rates indicate that the high strain rate may have the effect of increasing yield stress above the static yield value.

2.5. Temperature in Metal Cutting

During a metal cutting operation, high temperatures are generated because of plastic deformation of work piece material and friction along the tool/chip interface. Determination of temperatures in tool, chip and work piece is important for process efficiency because these temperatures have a great influence on the rate of tool wear,

strength of work piece material, mechanics of chip formation, surface integrity, cutting forces, etc.

Heat sources in metal cutting are shown in Figure 2.15. Heat source Q_1 occurs on shear plane due to intensive plastic deformation. The shear plane temperature is very important because it influences flow stress of work piece material and temperatures on the tool face.

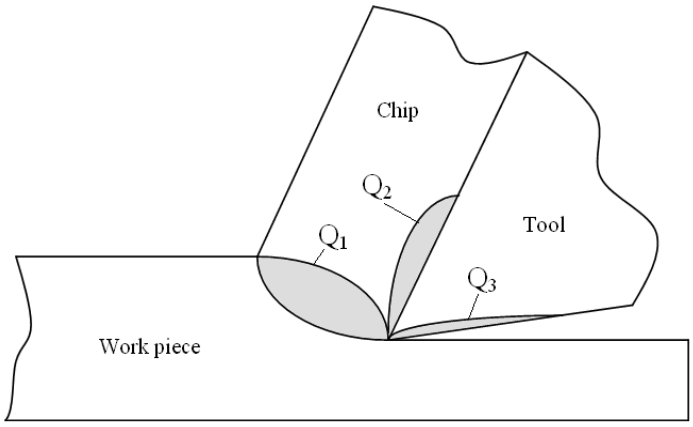

Figure 2.15. Locations of heat sources in metal cutting

Frictional heat source Q_2 localises at the tool-chip interface. Temperature of rake face is the maximum temperature in real machining operations and it causes tool wear. Another frictional heat source Q_3 is generated at the contact between the flank face of the tool and the work piece due to tip radius of the cutting tool.

Thermal studies in metal cutting have focused on determining the heat generation, its distribution in the cutting area and the maximum temperature. There are three types of methods used to achieve results about temperatures;

- Analytical: In the analytical studies, empirical correlations have been used to determine heat generation and temperature distribution. Analytical calculations have been done under simplified assumptions.
- Experimental: The experimental techniques such as thermo couple with tool/chip pair, thermal camera, etc. have been providing thermal distribution of cutting zone. Results of the experimental works mainly depend on calibration of the instruments used.
- Numerical: Distribution of temperature on the cutting zone has been obtained by using finite element, finite difference and boundary elements methods.

CHAPTER 3

FINITE ELEMENT SIMULATION OF METAL CUTTING

3.1. Introduction

Metal cutting researchers focus on determining the best cutting conditions and tool geometries for process efficiency. Experimental works are needed to obtain results but they are expensive and time consuming. In addition to this, simplified analytical methods have limited applications and they can not be used for complex cutting processes. At this point numerical methods become important. In last two decades, finite element method (FEM) has been most frequently used in metal cutting analysis. Various outputs and characteristics of the metal cutting processes such as cutting forces, stresses, temperatures, chip shape, etc. can be predicted by using FEM without doing any experiment. In this chapter, some basic aspects of finite element simulation of metal cutting are presented.

3.2. Model Formulation

Three main formulations are used in finite element simulation of metal cutting: Lagrangian, Eulerian and Arbitrary Lagrangian-Eulerian (ALE).

3.2.1. Lagrangian

Lagrangian formulation is mainly used in solid mechanics problems. Here the FE mesh is attached to work piece material and cover the whole of the region under analysis. This makes it highly preferable when unconstrained flow of material is involved. Lagrangian formulation is broadly used in metal cutting simulation due to ability to determine geometry of the chip from incipient stage to steady state and this geometry is a function of cutting parameters, plastic deformation process and material properties. Therefore, boundaries and shape of the chip do not have to be known a

priori. Besides, chip separation criteria can be defined to simulate discontinuous chips or material fracture in metal cutting models which are based on Lagrangian formulation.

Although there are many advantages of Lagrangian formulation, it has also shortcomings. Metal being cut is exposed severe plastic deformation and it causes distortion of the elements. Therefore, mesh regeneration is needed. Secondly, chip separation criteria must be provided. This drawback of formulation can be eliminated by using an updated Lagrangian formulation with mesh adaptivity or automatic remeshing technique.

3.2.2. Eulerian

In Eulerian formulation, the FE mesh is spatially fixed and the material flow through the control volume which eliminates element distortion during process. Besides, fewer elements required for the analysis, thereby reducing the computation time. Cutting is simulated from the steady state and therefore there is no need for separation criteria in Eulerian based models.

The drawback of Eulerian formulation is a need in determining the boundaries and the shape of the chip prior to the simulation. Also the chip thickness, the tool-chip contact length and the contact conditions between tool-chip must be kept constant during analysis which makes Eulerian formulation does not correspond to the real deformation process during metal cutting.

3.2.3. Arbitrary Lagrangian-Eulerian (ALE)

The best features of Lagrangian and Eulerian formulations have been combined and called arbitrary Lagrangian-Eulerian (ALE). In ALE formulation, the FE mesh is neither fixed spatially nor attached to the work piece material. The mesh follows the material flow and problem is solved for displacements in Lagrangian step, while the mesh is repositioned and problem is solved for velocities in Eulerian step.

The idea used in metal cutting simulation is to utilize Eulerian approach for modelling the area around the tool tip where cutting process occurs. Therefore, severe element distortion is avoided without using remeshing. Lagrangian approach is utilized for the unconstrained flow of material at free boundaries. Furthermore shape of the chip

occurs as a function of plastic deformation of the material. This approach is shown in Figure 3.1.

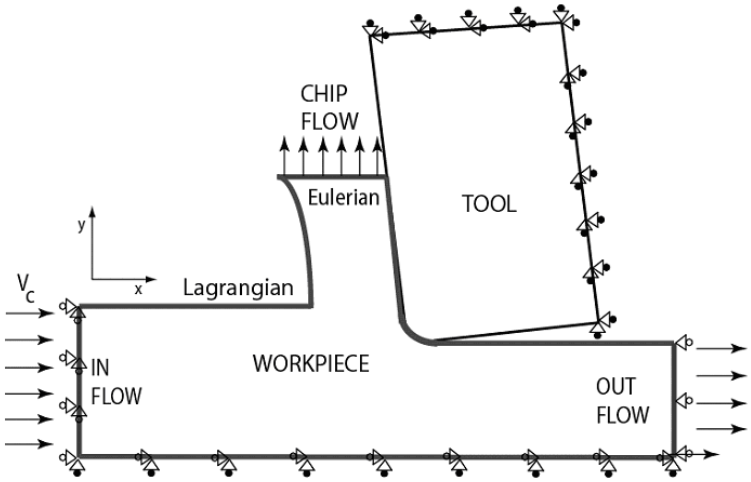

Figure 3.1. Eulerian and Lagrangian boundary conditions in ALE simulation (Source: Ozel, et al. 2007)

3.3. Meshing

A continuous region is divided discrete region called elements in FE analysis. This procedure is called discretization or meshing. Initial designed FE mesh can not hold its original shape and it is distorted due to severe plastic deformation during metal cutting or metal forming processes. The distortion causes convergence rate and numerical errors. To handle with this problem a new FE mesh must be generated in means of changing the size and distribution of the mesh. This is called adaptive mesh procedure.

One of adaptive mesh procedure is remeshing technique and it includes the generation of a completely new FE mesh out of the existing distorted mesh. Second one is called refinement technique which is based on increasing the local mesh density by reducing the local element size as shown in Figure 3.2.

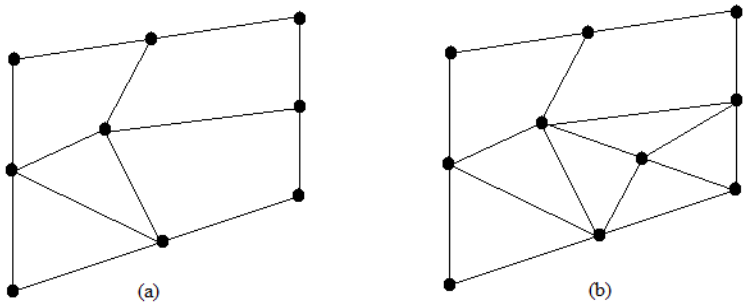

Figure 3.2. Refinement: (a) Initial local mesh, (b) Reducing element size

The last adaptive mesh technique is smoothing which includes reallocating the nodes to provide better element shapes as shown in Figure 3.3.

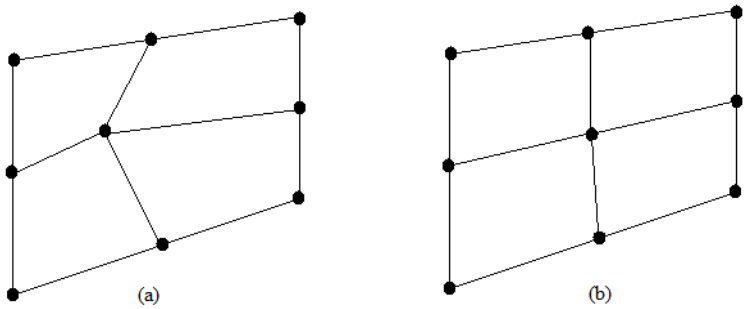

Figure 3.3. Smoothing: (a) Initial local mesh, (b) Reallocating of the nodes

The adaptive mesh procedure decreases solution errors during calculation therefore it increases the accuracy of the simulation. For these reasons, the adaptive mesh procedure must be used in FE simulations including severe plastic deformation such as metal cutting and metal forming.

3.4. Work Material Constitutive Models

One of the most important subjects in metal cutting simulation is modelling flow stress of work piece material properly in order to obtain true results. Flow stress is an instantaneous yield stress and it depends on strain, strain rate and temperature and represented by mathematical forms of constitutive equations. Among others, the most widely used ones in metal cutting simulations are Oxley, Johnson-Cook and Zerilli-Armstrong material constitutive models.

3.4.1. Oxley Material Model

Oxley (1990) and his co-workers used power law to represent material flow stress for carbon steel as

$$\sigma = \sigma_1 \varepsilon^n \tag{3.1}$$

Where σ and ε are flow stress and strain, σ_1 is the material flow stress at ε=1.0 and n is the strain hardening exponent. σ_1 and n depend on velocity modified temperature (T_{mod}) given by Macgregor and Fisher. T_{mod} is defined as

$$T_{\text{mod}} = T\left(1 - \nu \log \frac{\dot{\varepsilon}}{\dot{\varepsilon}_0}\right) \tag{3.2}$$

Where ν and $\dot{\varepsilon}_0$ are work piece material constants and they have values of 0.09 and 0.1 for carbon steel.

3.4.2. Johnson and Cook Material Model

Johnson and Cook (1993) developed a material model based on torsion and dynamic Hopkinson bar test over a wide range of strain rates and temperatures. This constitutive equation was established as follows:

$$\sigma = \left(A + B\varepsilon^n\right)\left(1 + C \ln \frac{\dot{\varepsilon}}{\dot{\varepsilon}_0}\right)\left(1 - \left(\frac{T - T_r}{T_m - T_r}\right)^m\right) \tag{3.3}$$

The first parenthesis is elastic-plastic term and it represents strain hardening. The second one is viscosity term and it shows that flow stress of material increases when material is exposed to high strain rates. The last one is temperature softening term. A, B, C, n and m are material constants that are found by material tests. T is instantaneous temperature, T_r is room temperature and T_m is melting temperature of a given material.

Johnson-Cook material model assumes that flow stress is affected by strain, strain rate and temperature independently.

3.4.3. Zerilli and Armstrong Material Model

Zerilli and Armstrong (1987) developed two micro structurally based constitutive equations. They worked on face-centred cubic (f.c.c.) and body-centred cubic (b.c.c.) metals to analyse their temperature and high strain rate responds and noticed a significant difference between these materials. Therefore, they developed two distinct models.

The constitutive equation for b.c.c. metals can be written as follows:

$$\sigma = C_0 + C_1 \exp\left(-C_3 T + C_4 T \ln\frac{\dot{\varepsilon}}{\dot{\varepsilon}_0}\right) + C_5 \varepsilon^n \tag{3.4}$$

Flow stress for f.c.c. metals is defined as

$$\sigma = C_0 + C_2 \varepsilon^{-1/2} \exp\left(-C_3 T + C_4 T \ln\frac{\dot{\varepsilon}}{\dot{\varepsilon}_0}\right) \tag{3.5}$$

In these equations, C_0 is component of stress that accounts for dislocation density on the flow stress, C_1 - C_5, n are material constants and T is the absolute temperature. In Equation 3.4, it is assumed that the strain dependence on flow stress is not affected by strain rate and temperature while it is opposite in Equation 3.5.

3.5. Friction Models

Friction modelling plays significant role on results such as cutting forces, temperature and tool wear in metal cutting simulation. Hence, researchers focused on determining a friction model to represent the real behaviour of process. The most widely used ones in metal cutting simulation can be listed as follows.

3.5.1 Constant Coulomb

In early metal cutting simulation, the simple Coulomb friction model was used on the whole contact zone with a constant coefficient of friction.

This model is defined as

$$\tau = \mu\sigma_n \tag{3.6}$$

Here, τ is the frictional stress, σ_n is the normal stress and μ is the coefficient of friction.

3.5.2 Constant Shear

In shear friction model, frictional stress on rake face of tool is assumed to be constant and the low stress variation of τ and σ_n are neglected.

This can be expresses by means of the following formulation:

$$\tau = mk \tag{3.7}$$

Where m is friction factor and k is shear flow stress of the work material.

3.5.3 Constant Shear in Sticking Zone and Coulomb in Sliding Zone

According to Zorev (1963), two friction regions occur on rake face of tool. The first region is sticking zone where the frictional stress is constant. The next one is sliding zone where the normal stress is small. Therefore, constant shear friction model in sticking zone and Coulomb's theory in sliding zone can be used to model friction phenomenon.

The important thing in using this model is to determine the length of sticking and sliding zones. According to Shatla, et al. (2001), it was assumed that the length of the sticking region was equal to two times of the uncut chip thickness. However, it was noticed that the sticking region covered all the contact length in this way. Thus, Ozel

(2006) suggested that the length of the sticking zone was equal to the uncut chip thickness.

3.6. Chip Separation Criteria

In real machining operations, continuous, discontinuous or segmented chips may occur. Two basic methods are used to provide real chip formation in a numerical method. Fist one is to define chip separation criteria along a pre-defined line and the next one is to use continuous remeshing which is based on large plastic deformation.

A number of separation criteria can be grouped as geometrical and physical. According to geometrical criteria, chip separation is started when the tool tip approaches a node along the parting line within a critical distance. Then that node is separated from the work piece and it becomes part of the chip. This process can be seen in detail in Figure 3.4. When distance D between the tool tip and node E becomes equal or less than the critical distance D_c, the connectivity of the Element 2 changes and a new node E' occur in that element. Then the node E moves upwards along EB by small distance, whilst node E' moves downwards by a small distance along E'G.

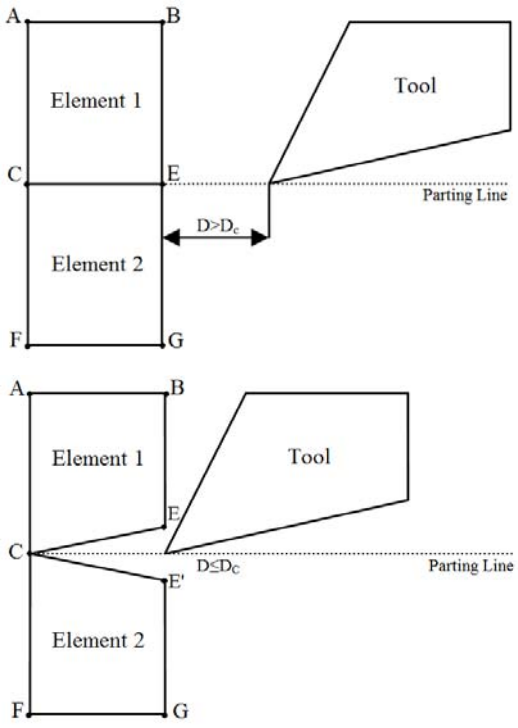

Figure 3.4. Geometrical Separation
(Source: Mamalis, et al. 2001)

This criterion is just based on geometrical considerations and the critical distance value is chosen arbitrarily. Because of that, it does not show real physical mechanism of chip formation. On the other hand chip separation can be easily controlled. In literature, Komvopoulos and Erpenbeck (1990) used this technique as chip separation criteria to model orthogonal metal cutting.

According to the physical criteria, separation of nodes occurs when the value of predefined critical physical parameter is reached at a node or element. This critic physical parameter can be selected as strain, stress or strain energy density depending on work material properties and cutting conditions.

Strenkowski and Carroll (1985) used effective plastic strain criterion to simulate orthogonal cutting. When the effective plastic strain at a node closest the tool tip is reached the predefined critical value, it is allowed to move from the work piece.

Physical criteria seem to be more accurate in modelling chip separation because they are based on work piece properties. However, the problem is to determine critical physical values for real process. For example, the strain energy of work piece material can be determined from a simple uniaxial tensile test of which mechanical conditions are significantly different from metal cutting. Therefore, using this value in modelling can not be reliable. Another example is using effective plastic strain. Effective plastic strain value changes significantly during the transition from transient to steady-state cutting and using this value as separation criterion can not act as a reliable criterion.

3.7. FE Software Packages and Utilization

Researchers usually wrote their own FE codes for specific process such as metal cutting analysis until the mid-1990s. In recent years, commercial FE packages such as Deform 2D/3D, Abaqus, Advantedge, Ls-Dyna and etc. have been used excessively in both academic and industrial world for process analysis. The choice of FE software for metal cutting analysis is very important for the quality of results. This is because different FE packages have different capabilities and solver techniques.

Deform, Design Environment for Forming, is a Finite Element Method based system that can be applied to several manufacturing processes such as forging, rolling and machining. Deform has a specific machining module to quickly set up turning, milling, boring and drilling operations. Tool-work piece geometry and cutting

conditions have to be supplied by the user. Additionally, software allows the user to adjust specific modelling variables such as mesh size, boundary conditions, and tool-work piece interface conditions. The program has a material library including different types of steel, super alloy, aluminium, titanium. New materials can be created by using material models.

Abaqus is a FE analysis program that can be used for variety of problems such as metal cutting as shown in Figure 3.5. Abaqus has not got a module for specific forming processes. Therefore, the user has to define tool and work piece geometries, cutting conditions, solver technique, boundary conditions and mesh size. This program has not got a material library but it allows the users to configure materials using variety of models. The significant advantage of using this software is to model a system with high level of detail. However, setting a setup for an analysis takes a lot of time and the user has to be experienced.

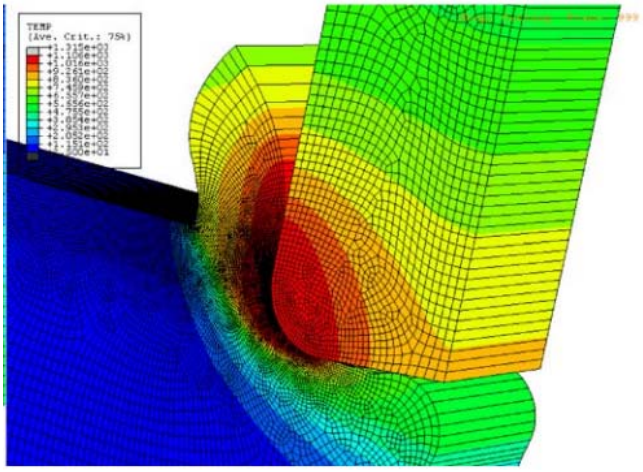

Figure 3.5. Orthogonal metal cutting simulation by using Abaqus
(Source: Ozel, et al. 2007)

Advantedge was developed for metal cutting operations such as turning, milling, drilling as shown in Figure 3.6. The software has got simple input interfaces to supply work piece and tool geometries as well as the cutting conditions. Advantedge also has extensive material library. The user control on solver and material inputs are not allowed in this program.

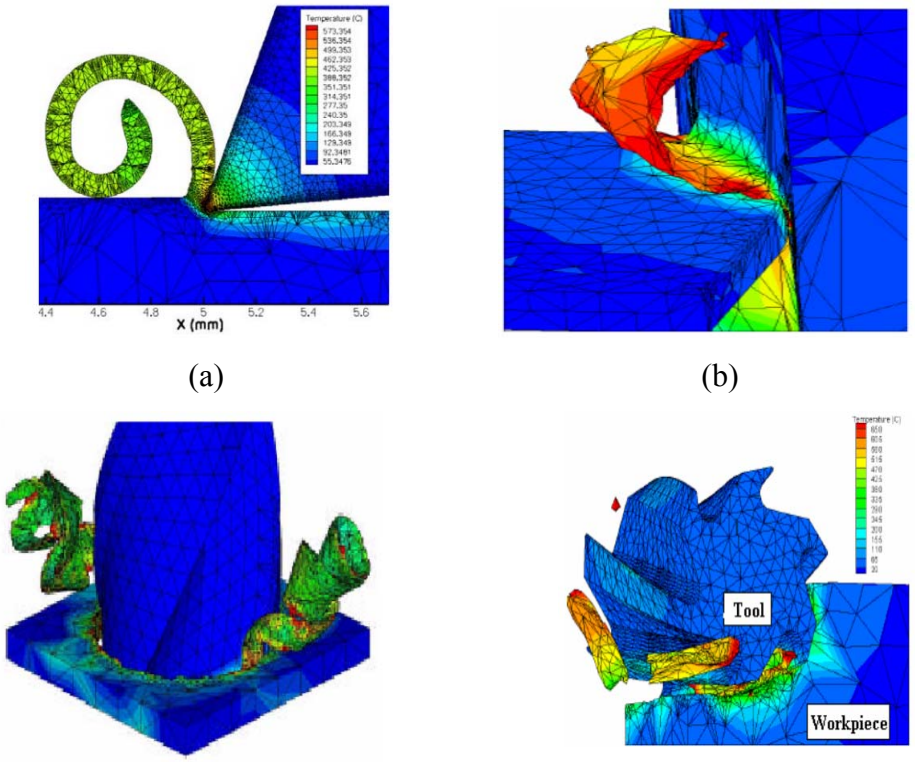

(a) (b)

(c) (d)

Figure 3.6. Modelling by using Advantedge; (a) 2D Turning, (b) 3D Turning, (c) Drilling, (d) Cylindrical Milling (Source: Petrarius, et al. 2008)

Ls-Dyna is an explicit and implicit finite element program used to analyze safety analysis and crash, forming problems. Ls-Dyna can be used for metal cutting simulations as shown in Figure 3.7. However, this program does not include machining module and it is time consuming to model metal cutting operations. In addition to this, Ls-Dyna does not have ability to do remeshing at tool and work piece contact area affecting the results in metal cutting simulations.

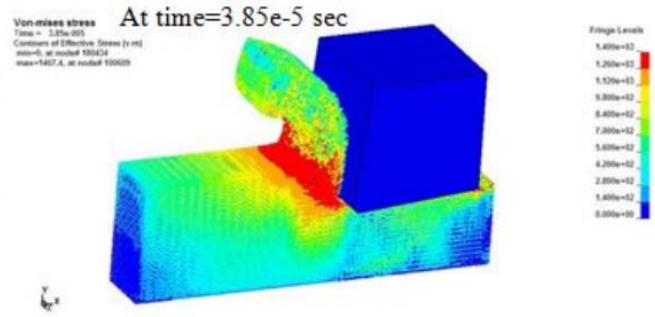

Figure 3.7. Metal cutting simulation with by using Ls-Dyna (Source: Ambati 2008)

CHAPTER 4

PRESENT MODEL AND SIMULATION OF METAL CUTTING

4.1. Introduction

The modelling part of metal cutting simulation is very important step to achieve accurate results. In this chapter, details of modelling tool, work piece and cutting system are presented.

4.2. Tool Modelling

In analysis, cutting tool is assumed to be a rigid body. Geometric variables of the tool are given in Table 4.1.

Table 4.1. Geometric variables of the cutting tool
(Source: Filice, et al. 2007)

Rake Angle, α (º)	Clearance Angle, c (º)	Tip Radius, r_T (mm)
0	4	0.05

Tool material was selected uncoated tungsten carbide (WC). Thermal and mechanical properties of WC are given in Table 4.2.

Table 4.2. Thermal and mechanical properties of WC

Elastic Modulus, E (MPA)	650000
Poisson's Ratio	0.25
Thermal Expansion (1/ºC)	5.10^{-6}
Thermal Conductivity (N/sec/ºC)	50
Heat Capacity (N/mm^2 ºC)	4

Finite element mesh of tool is modelled using 1185 nodes and 1127 elements. Iso-parametric quadrilateral elements are used for the analysis. The distribution of mesh on tool is not uniform. Mesh density of tool tip and a part of rake face are modelled high with using mesh windows in the software to obtain more accurate temperature distribution results. This design is shown in Figure 4.1.

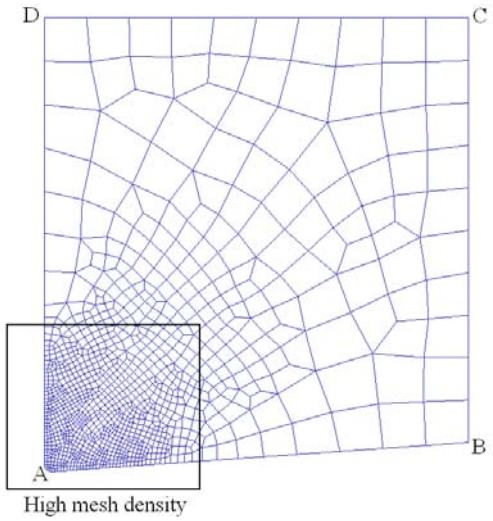

Figure 4.1. Mesh design of the tool

Heat exchange is defined on the boundaries D-A and A-B. Boundaries B-C and D-C are sufficiently away from cutting edge therefore their temperature is fixed 20 ºC.

4.3. Work piece Modelling

Flow stress modelling of work piece material is very important to achieve satisfactory results from metal cutting simulation. In the analysis, AISI 1045 is selected as work piece material. Oxley, Johnson-Cook and Zerilli-Armstrong material constitutive models are used to model the plastic behaviour of AISI 1045. Due to high strain, strain rate and temperature in metal cutting, the material data is represented by flow curves at 11 different strain (0.05, 0.5, 1, 1.5, 2, 2.5, 3, 3.5, 4, 4.5, 5), 7 different strain rates (1, 10, 100, 1000, 10000, 100000, 500000 s^{-1}) and 7 different temperature (20, 100, 300, 500, 700, 900, 1200 ºC).

Material coefficients listed in Table 4.3. and Table 4.4. are used in calculating Johnson-Cook and Zerilli-Armstrong flow stress values.

Table 4.3. Constants for Johnson-Cook constitutive model
(Source: Jaspers ,et al. 2002)

A [MPa]	B [MPa]	C (-)	n (-)	m (-)	T_m (K)
553.1	600.8	0.0134	0.234	1	1733

Table 4.4. Constants for Zerilli-Armstrong constitutive model
(Source: Jaspers, et al. 2002)

C_o [MPa]	C_1 [MPa]	C_3 (K^{-1})	C_4 (K^{-1})	C_5 (MPa)	n (-)
159.2	1533.7	0.00609	0.000189	742.6	0.171

Examples of flow curves for each material constitutive model are shown in Figure 4.2.-4.10.

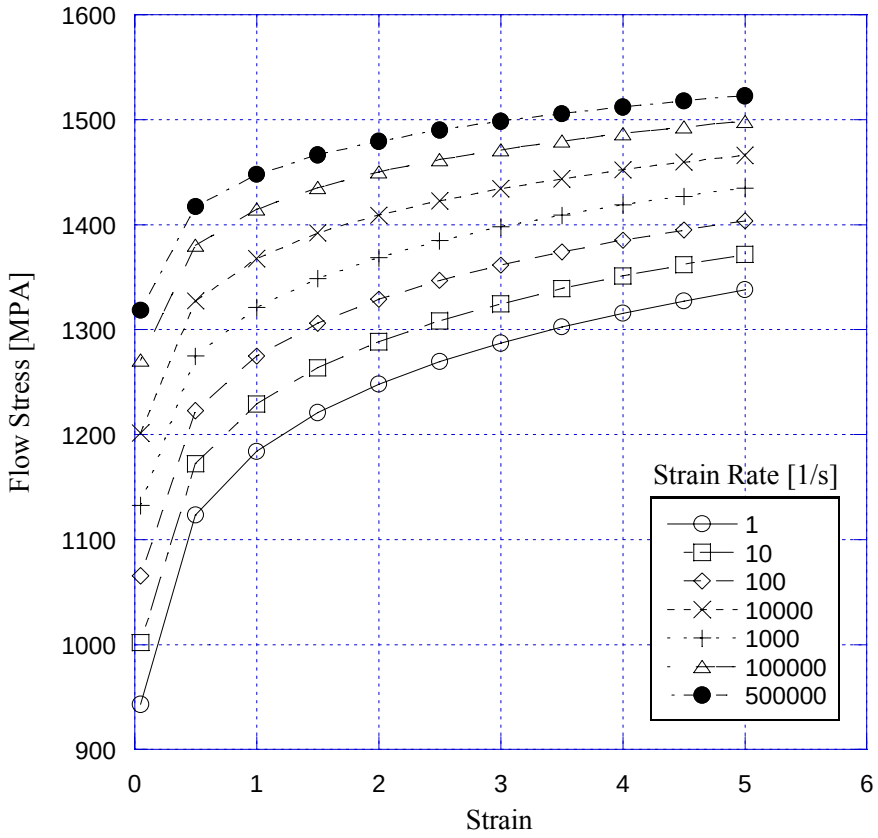

Figure 4.2. AISI 1045 Oxley flow curve at T=20 ºC

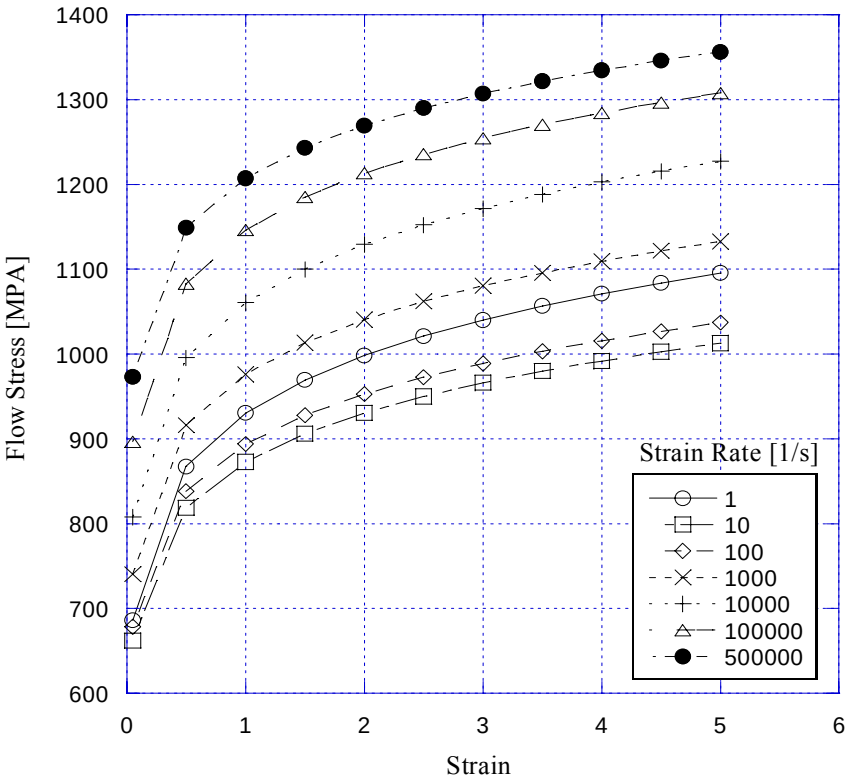

Figure 4.3. AISI 1045 Oxley flow curve at T=300 ºC

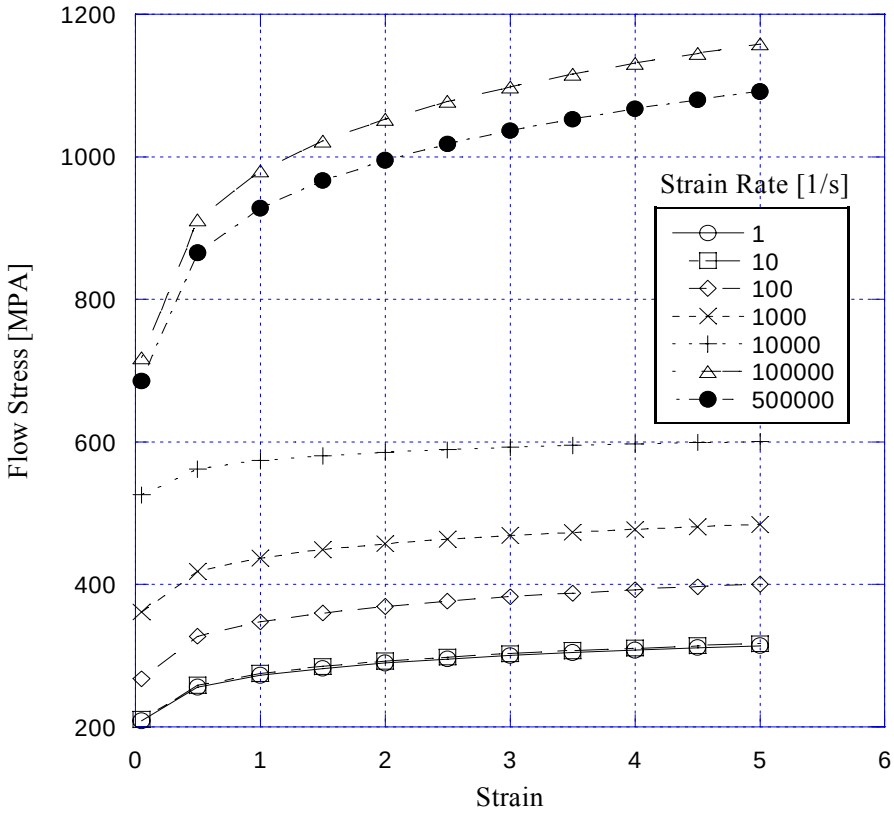

Figure 4.4. AISI 1045 Oxley flow curve at T=900 ºC

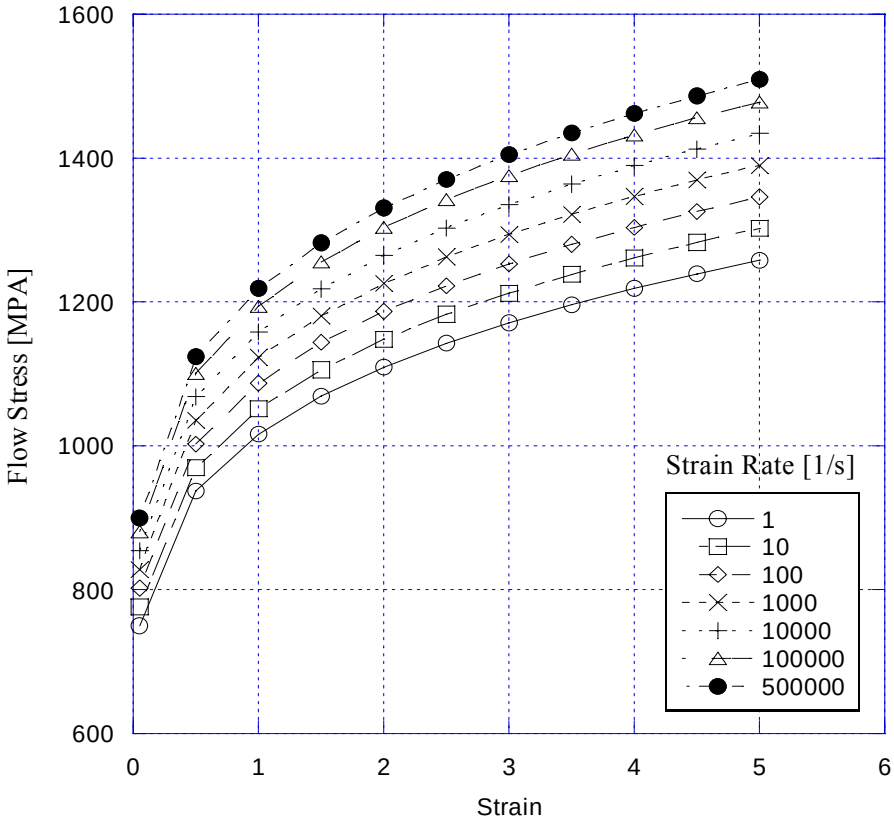

Figure 4.5. AISI 1045 Johnson-Cook flow curve at T=20 ºC

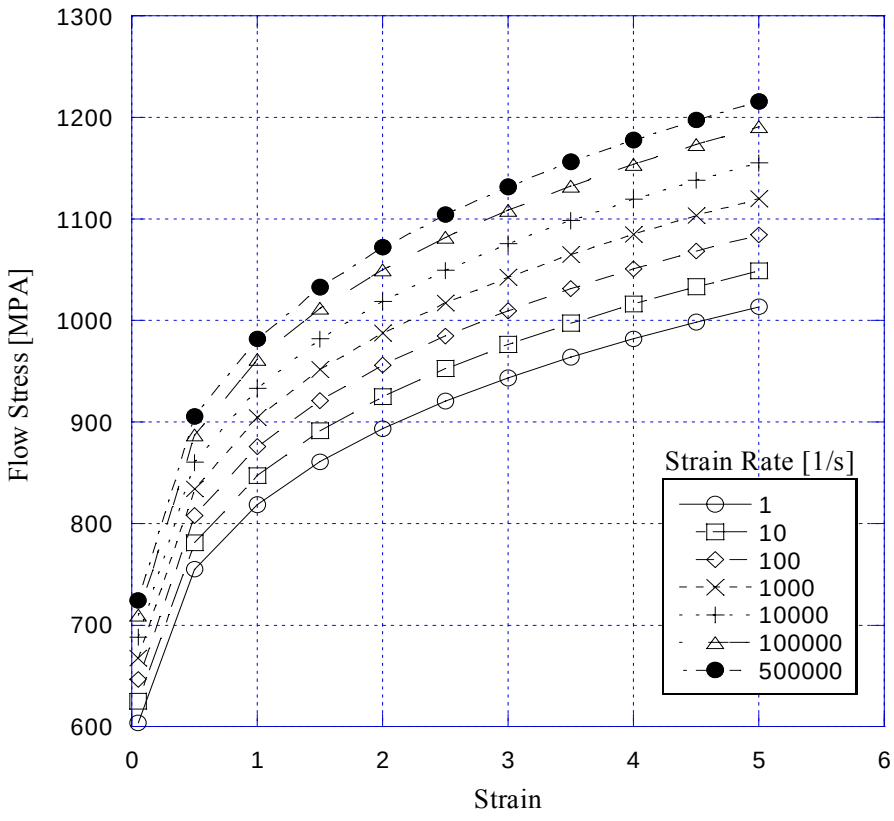

Figure 4.6. AISI 1045 Johnson-Cook flow curve at T=300 ºC

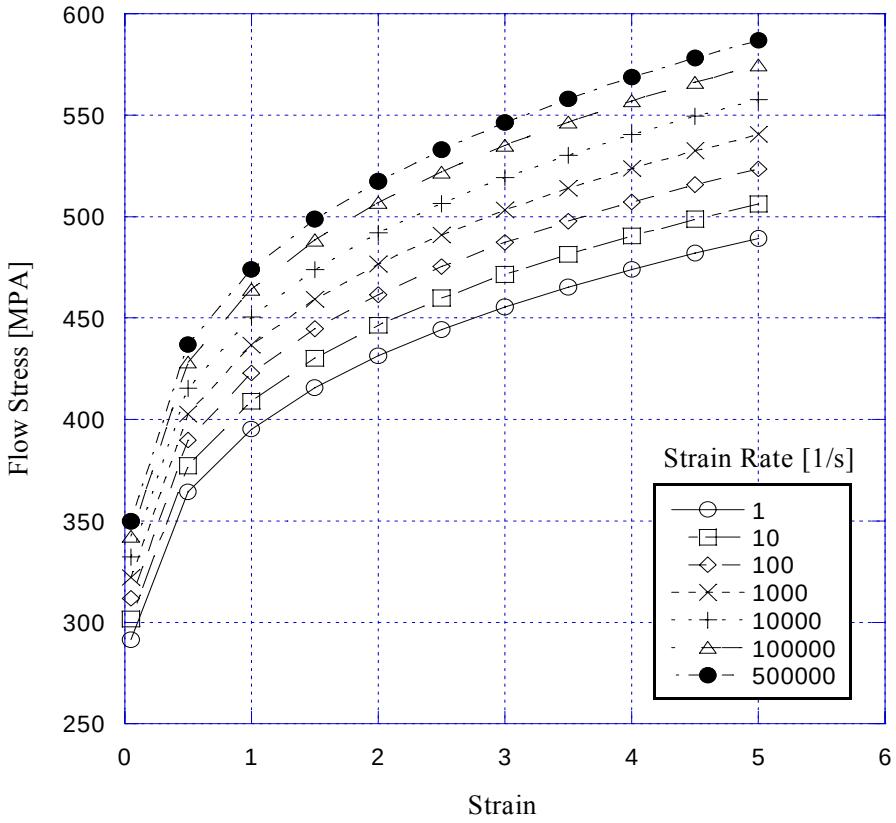

Figure 4.7. AISI 1045 Johnson-Cook flow curve at T=900 ºC

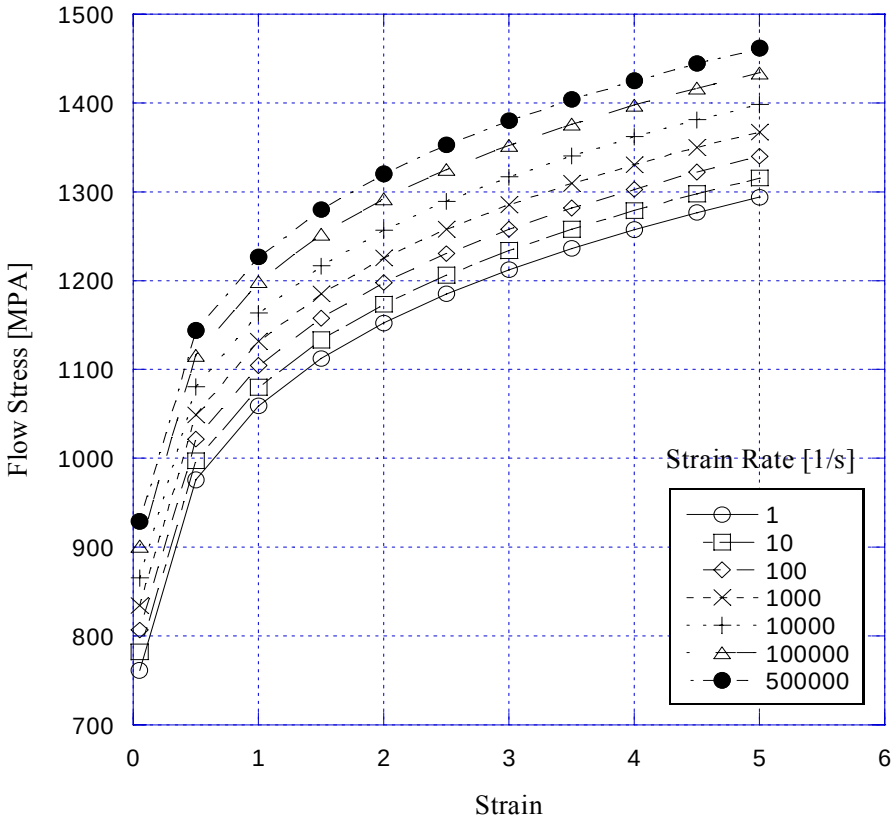

Figure 4.8. AISI 1045 Zerilli-Armstrong flow curve at T=20 ºC

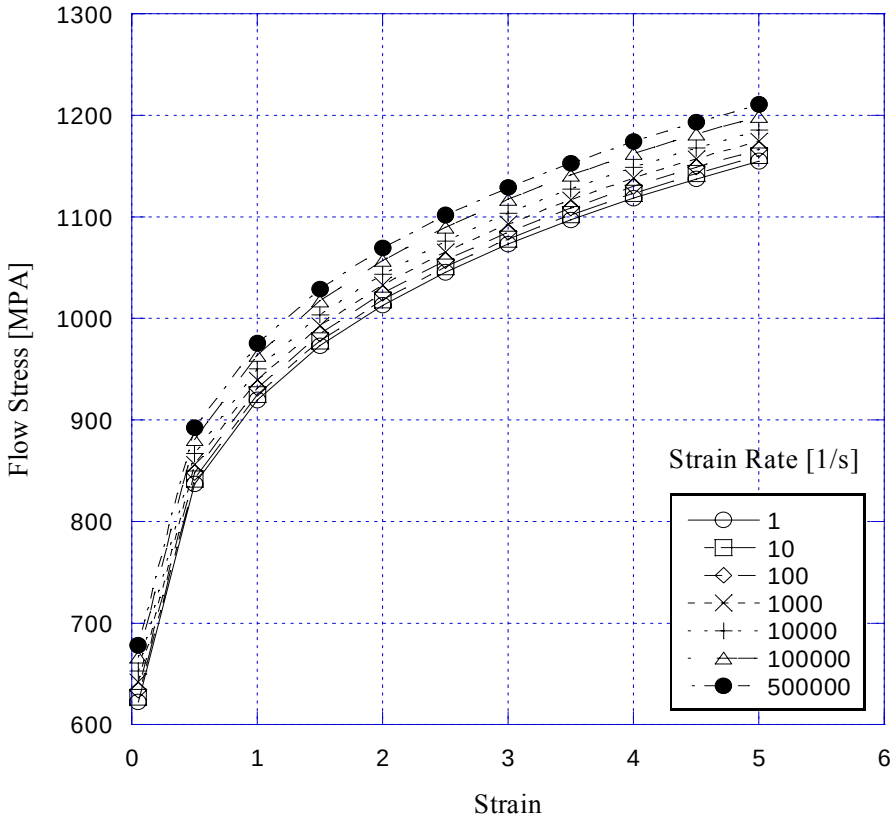

Figure 4.9. AISI 1045 Zerilli-Armstrong flow curve at T=300 ºC

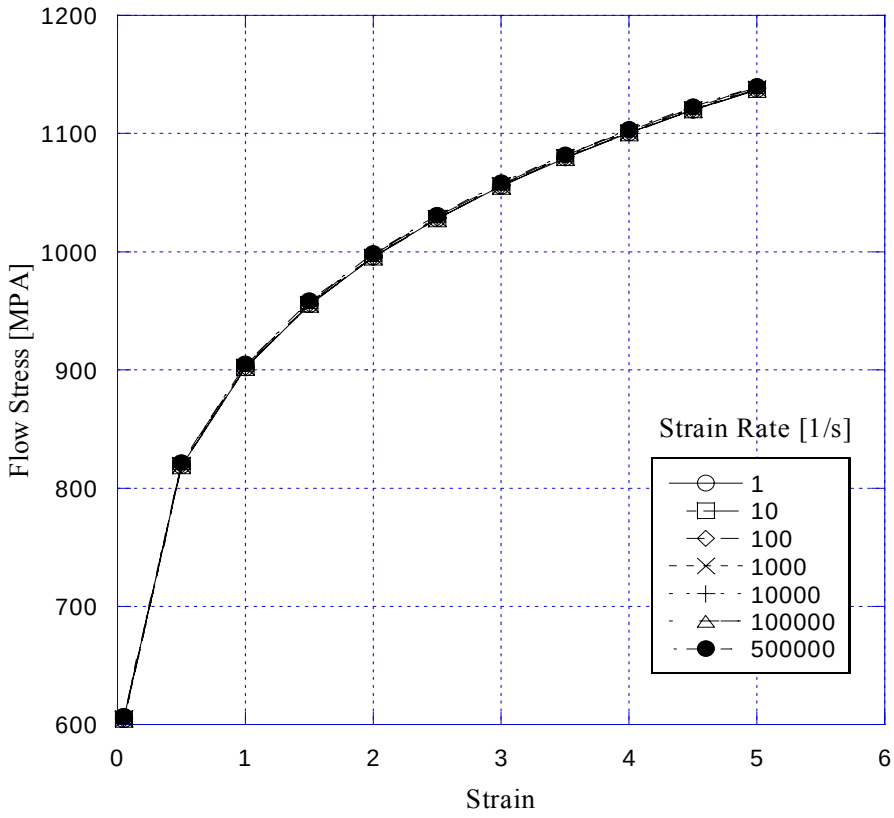

Figure 4.10. AISI 1045 Zerilli-Armstrong flow curve at T=900 ºC

During analysis, it is assumed that work piece does not undergo elastic deformation and it is allowed to show only plastic behaviour.

Finite element mesh of work piece is modelled using 3130 nodes and 3005 iso-parametric quadrilateral elements. The work piece is created at least 20 feeds long and 10 feeds high therefore the predicted results are not sensitive to the displacement boundary conditions and steady state can be reached. Mesh of deformation zone is modelled very dense as shown in Figure 4.11. in order to reduce calculation time and obtain more accurate results.

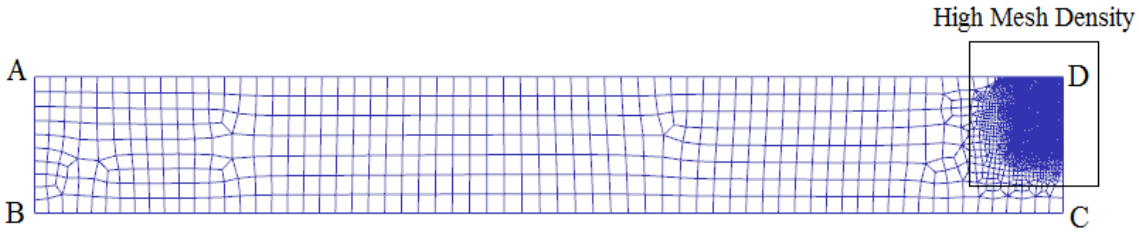

Figure 4.11. Mesh design of the work piece

Heat exchange is defined on the boundaries A-D and D-C. Boundaries A-B and B-C are sufficiently away from cutting edge therefore their temperature is fixed 20 ºC.

In addition to plastic properties of work piece, its thermal properties depending on temperature have to be given to the software for heat transfer calculation. Thermal conductivity, thermal expansion and heat capacity of AISI 1045 are shown in Figure 4.12., Figure 4.13. and Figure 4.14.

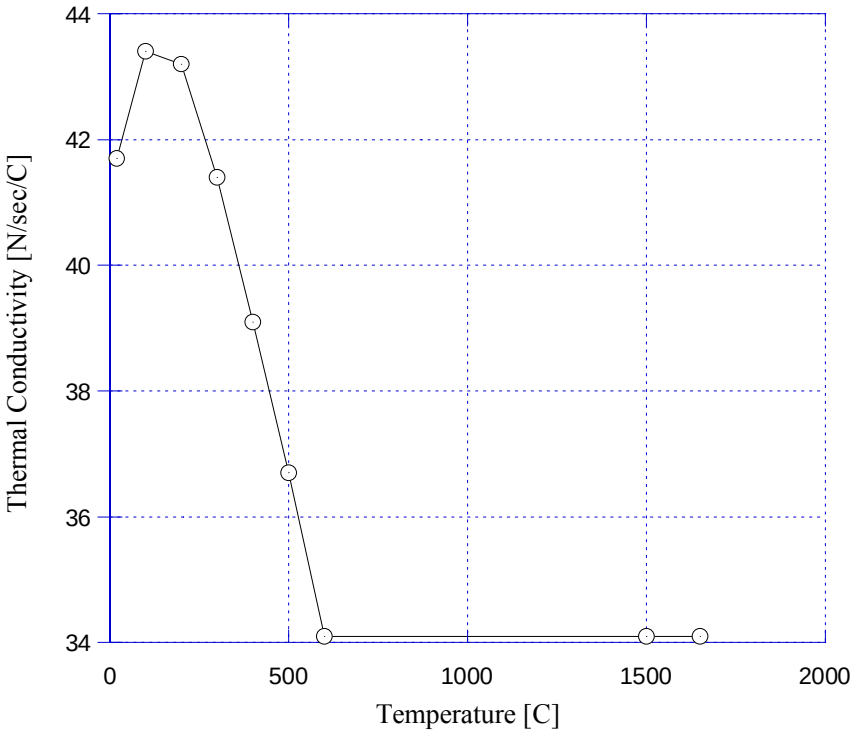

Figure 4.12. Thermal Conductivity of AISI 1045

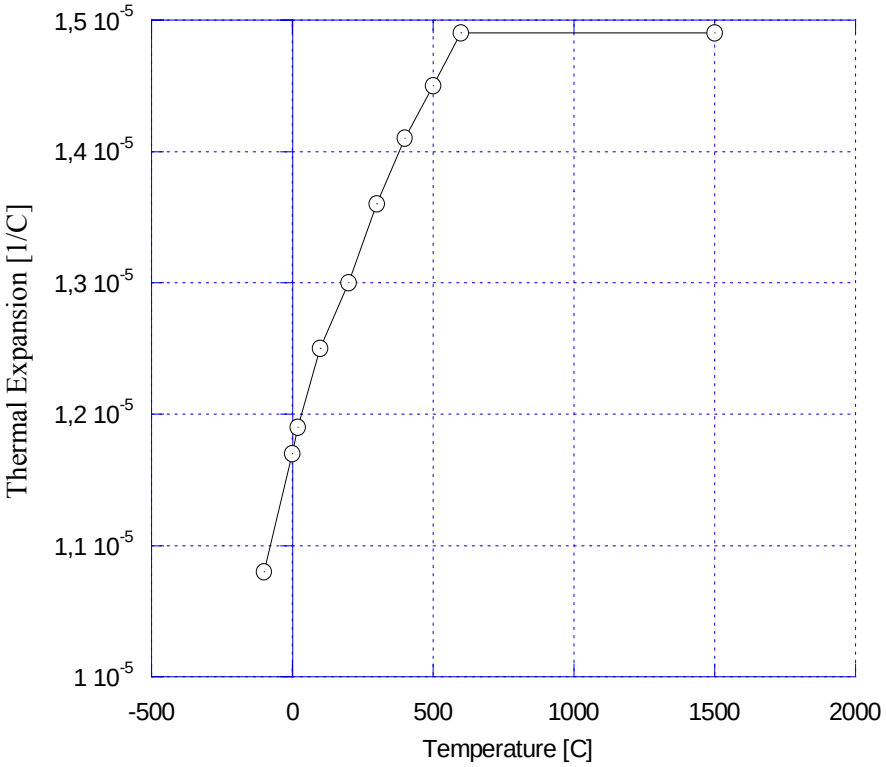

Figure 4.13. Thermal Expansion of AISI 1045

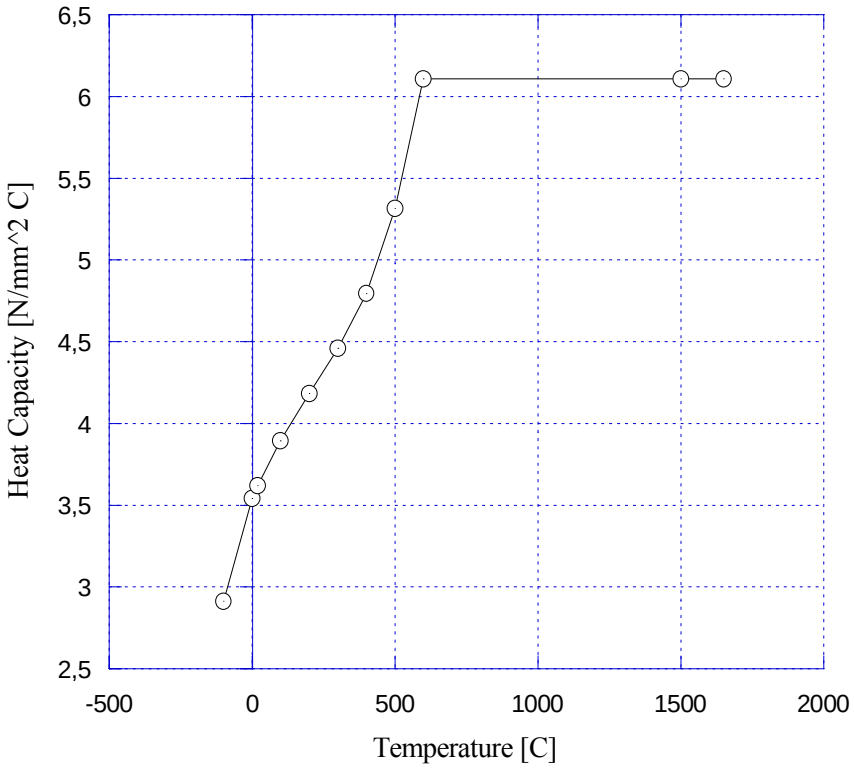

Figure 4.14. Heat capacity of AISI 1045

4.4. System Modelling

After modelling metal cutting components one by one, the next step is to assembly them due to cutting conditions. Cutting conditions are shown in Table 4.5.

Table 4.5. Cutting conditions
(Source: Filice et al., 2007)

Cutting Velocity, V_c (m/min)	Feed Rate, f (mm/rev)	Width of Cut, b (mm)
100	0.1	3

Displacement boundary conditions of the system are shown in Figure 4.15. The tool is supported by fixing the nodes on the boundary C-D-E in both x and y direction. The work piece is fixed at y direction and it is moved against the tool by applying a constant cutting velocity at the bottom boundary A-B.

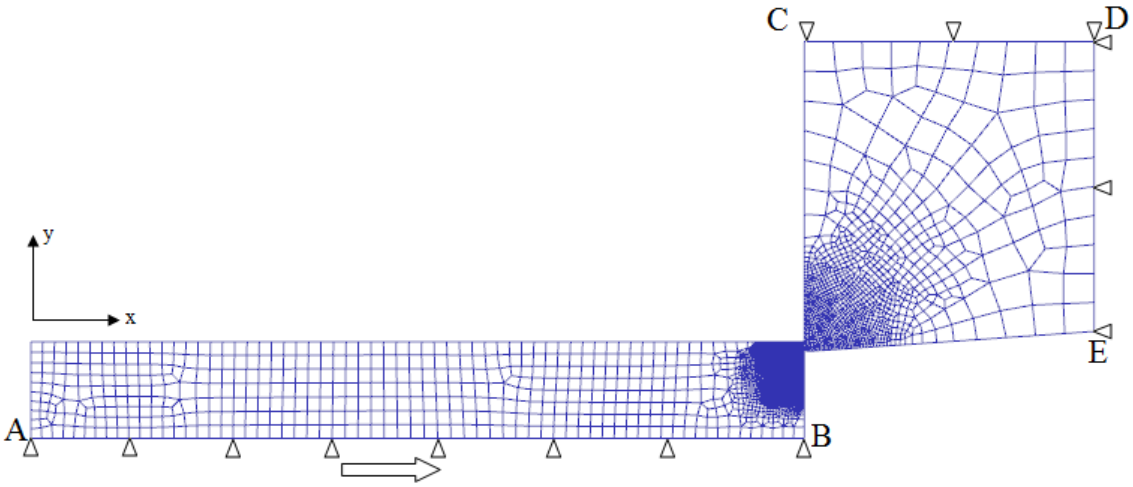

Figure 4.15. Displacement boundary conditions of the cutting system

For the heat transfer calculations, the following assumptions are made:

i) The contact between the tool and the chip is thermally perfect. Hence a very large value of the interface heat transfer coefficient (h_{int}) is used and it is fixed to 1000 kW/m^{2}K (Filice, et al. 2007).

ii) The boundaries that are sufficiently away from the cutting zone remain at the room temperature (T_∞=20 ºC)

iii) The chip and the tool loss heat due to heat convection (h_∞=20 W/m^2 ºC) on the free surfaces on the work piece.

iv) Heat loss due to radiation is very small and it is neglected.

Thermal boundary conditions of the system can be defined as

$$
\begin{aligned}
T &= T_\infty && (\text{on } S_T)\\
-k\frac{\partial T}{\partial n} &= h_{\text{int}}\left(T - T_C\right) && (\text{on } S_C)\\
-k\frac{\partial T}{\partial n} &= h_\infty\left(T - T_\infty\right) && (\text{on } S_H)\\
-k\frac{\partial T}{\partial n} &= 0 && (\text{on } S_o)
\end{aligned}
\qquad (4.1)
$$

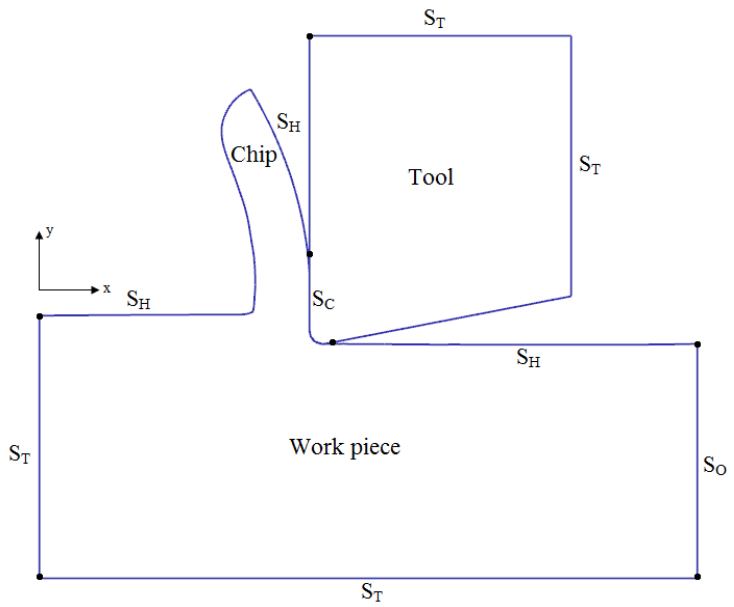

Figure 4.16. Thermal boundary conditions of the cutting system

Another important step is to define contact between the work piece and the tool. The tool is selected as master object because it was defined as a rigid object. The work piece is defined as slave object. Then, friction type, friction coefficient and interface heat transfer coefficient is defined. Therefore, contact is generated as shown in Figure 4.17.

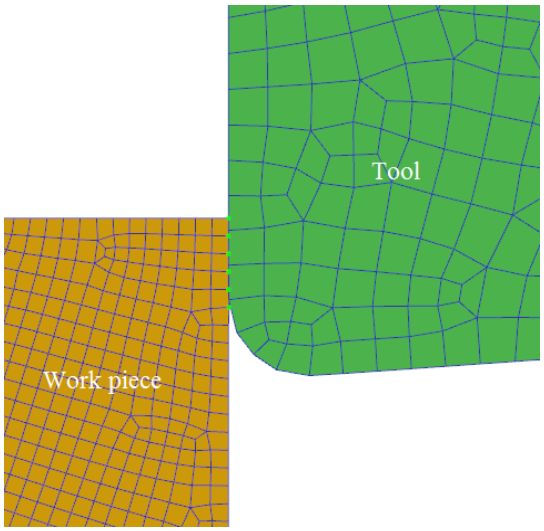

Figure 4.17. Contact generation between the tool and the work piece

In the analysis, updated Lagrangian model formulation with automatic remeshing method is used. Chip flow is achieved by remeshing hence there is no need

to use a separation criterion. When element distortion is detected, mesh generation is started as shown in Figure 4.18. Remeshing module will divide the contact boundary, add up suitable internal node or smooth elements and then interpolate stress, strain data for new mesh. As a second, plain strain assumption is made.

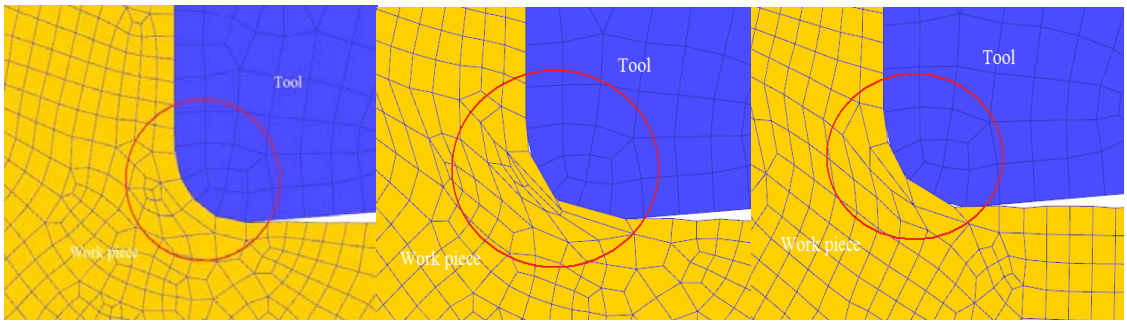

(a) (b) (c)

Figure 4.18 Remeshing procedure at cutting zone; (a) Initial mesh distribution, (b) Mesh distortion, (c) New mesh generation.

CHAPTER 5

RESULTS AND DISCUSSION

5.1. Introduction

In this chapter, the results of finite element simulations are presented. Firstly, simulation results and experimental results available in the literature are compared. Secondly, mechanical and thermal parameters of cutting such as strain, strain rate, stress and temperature are investigated.

Experimental results are given in Table 5.1. as follows;

Table 5.1. Experimental results
(Source: Filice, et al. 2007)

Cutting Force, F_c (N)	745
Thrust Force, F_t (N)	600
Contact Length, L_c (mm)	0.5
Chip thickness, t_c (mm)	0.29
Shear Angle, Ø (º)	19
Temperature, T (ºC)	542

5.2. Comparison of Material Constitutive Models

As mentioned, three different constitutive models are used in this study. Three simulations are carried out with using same friction model and coefficient. Friction coefficient is calculated by using Equation 2.15 and it is equal to 0.8053.

Effect of material constitutive models on cutting and thrust force is given in Table 5.2. It can be stated that Oxley model can predict cutting force more accurate in contrast to other two. All models overestimate cutting force.

Table 5.2. Cutting force and thrust force results for different material models

	Oxley	Johnson-Cook	Zerilli-Armstrong
F_c [N]	855	918	1224
F_t [N]	522	570	792

Thrust force is underestimated when using Oxley and Johnson-Cook models. However, it is overestimated when using Zerilli-Armstrong model.

It can be seen that cutting and thrust forces are depending on flow stress models. Some error occurred in the analysis when calculating forces. The differences between the experimental and predicted cutting force may be attributed to rigid tool and simplified friction model with constant coefficient usage in simulations. Secondly, measurement errors in experiments may be taken into consideration. Above considerations are valid when discussing thrust force errors too. In addition to them, thrust force is strongly affected by the state of machined surface, tool wear and the elastic recovery of the work piece (Kim, et al. 1999). In this model none of them are considered.

Table 5.3. shows the results of chip geometry results. Chip thickness and contact length between the rake face of the tool and the work piece are best estimated when Oxley model is used. High error occurs in calculating contact length when using Johnson-Cook and Zerilli-Armstrong models.

Value of experimental shear angle is calculated using Equation 2.5. Shear angle estimated by Johnson-Cook and Zerilli-Armstrong model is good agreement with the experimental value. Oxley model overestimated shear angle.

Table 5.3. Chip geometry results for different material models

	Oxley	Johnson-Cook	Zerilli-Armstrong
t_c [mm]	0.24	0.36	0.5
L_c [mm]	0.54	1.32	1.55
Ø [º]	25	20	16.7

Temperature predictions are shown in Table 5.4. Predicted temperature in metal cutting simulation is mainly affected by friction models, friction coefficients, interface heat transfer coefficient and accuracy of thermal parameters of tool and work piece. It

can be stated that flow stress models can affect temperature predictions too. All flow stress models give reasonable results.

Table 5.4. Temperature results for different material models

	Oxley	Johnson-Cook	Zerilli-Armstrong
T [ºC]	522	490	603

5.3. Comparison of Friction Models

In this part of the study, Shear and Coulomb friction models with constant coefficients are firstly implemented in finite element model. Then, a hybrid model, constant Shear friction in sticking zone and constant Coulomb friction in sliding zone, is used. For each of them, different coefficients are tested in order to find the value that better fits the experimental results. Oxley's material constitutive model is used in all simulations.

Firstly, constant shear friction model is used in finite element simulations. Table 5.5. shows chip geometry results. It can be seen that chip thickness, contact length and shear angle are best estimated when friction factor, m, is taken as 0.8053. Simulation results tend to close to the experimental results with increasing friction factor.

Table 5.5. Effect of shear friction factors on the chip geometry

Friction Factor	t_c [mm]	L_c [mm]	Ø [º]
0.6	0.21	0.234	27
0.7	0.22	0.29	26
0.8053	0.24	0.54	25

Effect of shear friction factors on cutting and thrust force is shown in Table 5.6. Cutting force is overestimated when shear friction factor is taken as 0.7 and 0.8053. Best estimated value is 741 N when shear friction factor is equal to 0.6. All thrust force results are underestimated. It is best estimated when shear friction factor is taken as 0.8053.

Table 5.6. Effect of shear friction factors on cutting and thrust force

Friction Factor	F_c [N]	F_t [N]
0.6	741	411
0.7	780	453
0.8053	855	522

Table 5.7. shows the predicted temperature with varying shear friction factors. All of them are underestimated. Possible reason for this difference may be due to the fact that the process temperature is obtained for a very short cutting time, which is not sufficient to reach steady state temperature. It can be noted that the best prediction is obtained when shear friction factor is equal to 0.8053.

Table 5.7. Effect of shear friction factors on temperature

Friction Factor	T [ºC]
0.6	453
0.7	478
0.8053	522

Secondly, constant Coulomb friction model is used on the whole tool-chip interface in finite element simulations. Chip thickness and shear angle are best estimated when friction coefficient is taken as 0.6. It is interesting to note that contact length is very sensitive to friction coefficient. It is best estimated when μ=0.6.

Table 5.8. Effect of Coulomb friction coefficients on the chip geometry

Friction Coefficient	t_c [mm]	L_c [mm]	Ø [º]
0.5	0.24	0.3	24
0.6	0.27	0.685	23

Table 5.9. shows cutting and thrust force predictions with different Coulomb friction coefficients. Cutting force is overestimated. Although thrust force is underestimated when friction coefficient is taken as 0.5, it is overestimated when μ=0.6.

Table 5.9. Effect of Coulomb friction coefficients on cutting and thrust force

Friction Coefficient	F_c [N]	F_t [N]
0.5	870	564
0.6	915	624

Temperature predictions are shown in Table 5.10. Temperature is sufficiently well estimated when friction coefficient is equal to 0.5.

Table 5.10. Effect of Coulomb friction coefficients on temperature

Friction Coefficients	T [ºC]
0.5	555
0.6	623

Lastly, a hybrid model consisting of Shear and Coulomb friction models is used. Length of sticking zone is assumed to be equal to two times of uncut chip thickness as proposed by Shatla, et al. (2001) and Shear friction model is applied to this region. Coulomb friction model is applied to rest of the contact interface. Two different shear friction factors and three different Coulomb friction coefficients are used in the analysis as listed in Table 5.11. These values are determined using previous analysis.

Table 5.11. Constant shear friction in sticking zone and Coulomb friction model in sliding zone (Hybrid Model)

Model Number	Shear friction factor-Coulomb friction coefficient
1	m=0.7 - μ=0.6
2	m=0.8 - μ=0.4
3	m=0.8 - μ=0.5
4	m=0.8 - μ=0.6

Chip geometry results are reported in Table 5.12. It can be seen that chip thickness and shear angle are best estimated when using model 4. It is also observed that contact length is more sensitive to Coulomb friction coefficient than shear friction factor.

Table 5.12. Effect of hybrid friction model on chip geometry

Model Number	t_c [mm]	L_c [mm]	Ø [º]
1	0.22	0.37	25
2	0.25	0.58	24
3	0.26	0.7	23
4	0.28	1.11	23

Table 5.13. shows cutting and thrust force predictions. All cutting force results are overestimated. The best value of cutting force is predicted when using model 1. Thrust force is underestimated when using model 1 and 2. Model 3 gives thrust force 600 N which equals to experimental value. Model 4 overestimates thrust force.

Table 5.13. Effect of hybrid friction model on cutting and thrust force

Model Number	F_c [N]	F_t [N]
1	831	482
2	906	588
3	912	600
4	927	621

Temperature predictions are shown in Table 5.14. All models underestimate temperature. There is not a significant difference between models in the view of results.

Table 5.14. Effect of hybrid friction model on temperature

Model Number	T [ºC]
1	390
2	414
3	412
4	414

5.4. Analysis of Mechanical and Thermal Parameters

In this part of the study, the distribution of strain, strain rate, stress and temperature in the deformation zone, which are hard to measure experimentally, are proposed. In the analysis, Oxley's material constitutive model and Shear friction model are used. Mesh of work piece consists of 4938 nodes and 4792 iso-parametric quadrilateral elements. All parameters are collected after a 3 mm tool stroke where steady state has reached.

First analysis is carried out with 0º rake angle as pervious works. The distribution of temperature in the work piece, chip and tool are shown in Figure 5.1. The maximum temperature is located on the secondary shear zone due to friction between the chip and the rake face of the tool. The highest temperature in the tool is achieved just above the tool tip.

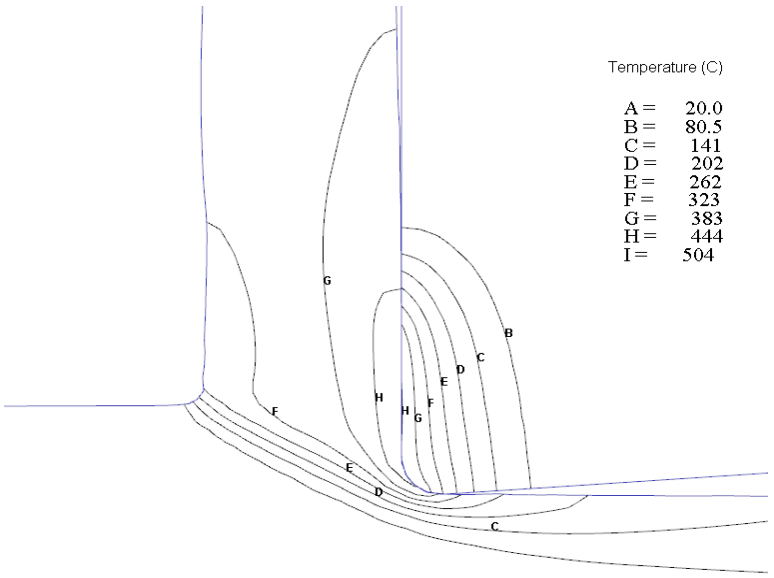

Figure 5.1. Temperature distribution

Plastic strain is shown in Figure 5.2. It can be seen that as an element of the work piece passes though the deformation zones, its magnitude of plastic strains increases. High plastic strain appears in the secondary shear zone where the maximum temperatures are located, with a maximum value of 2.85 and it remains constant away from the deformation zone. High plastic strains are also observed underneath the machined surface with the maximum value of 1.22. Plastic strain value is also equal to

1.22 in the primary shear zone. This value is smaller in contrast to plastic strain in the secondary shear zone due to high strain hardening and low temperature in this area.

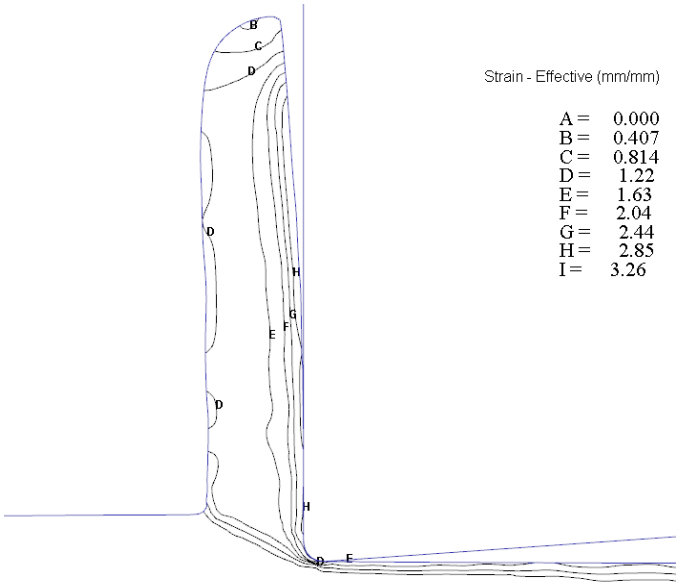

Figure 5.2. Plastic strain distribution

Strain rate distribution is presented in Figure 5.3. High strain rates are obtained along the primary shear zone which is a very small area. The maximum value of about 4.10^4 s^{-1} is obtained at the ahead of the tool tip. Strain rate starts to decrease gradually from the tool tip then it remains almost constant in the shear zone.

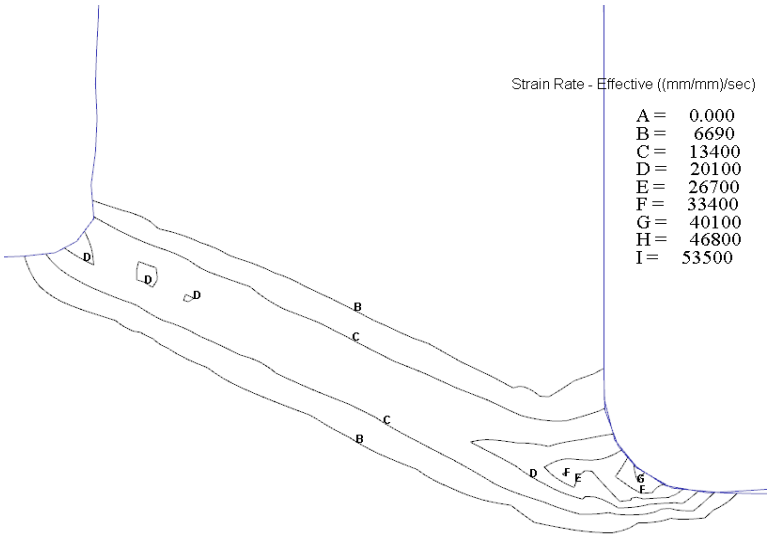

Figure 5.3. Strain rate distribution

Effective stress distribution is shown in Figure 5.4. It can be seen that effective stress reaches the maximum value at the primary shear zone due to increase in both strain and strain rate. Then it starts to decrease towards the secondary shear zone due to decrease in strain rate and increase in temperature. A maximum value of 1060 MPa is obtained in the primary shear zone and 911 MPa in the secondary shear zone.

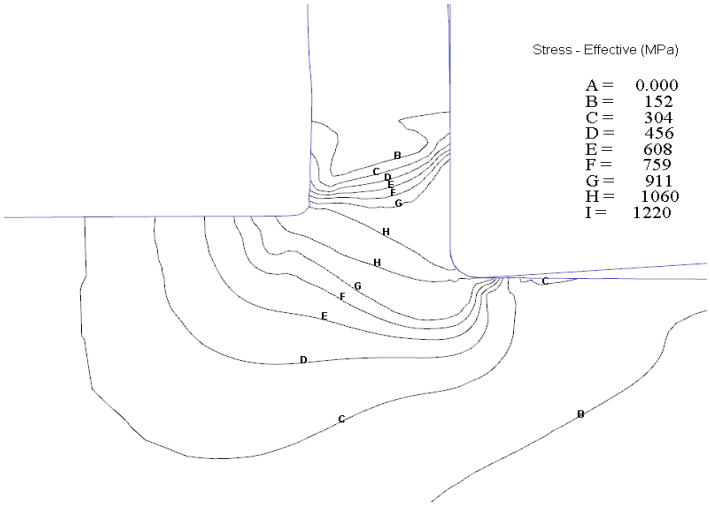

Figure 5.4. Effective stress distribution

5.5. Effects of Rake Angles

In this part of the study, effects of rake angle on the distribution of strain in work piece and the distribution of stress and temperature in both work piece and tool are analysed. In the analysis, three different rake angles (-10º, 0º, 10º) are used.

The effects of different rake angles on strain distribution are shown in Figure 5.5., Figure 5.6. and Figure 5.7. When rake angle becomes negative, strain in the chip increases because of larger contact length between the chip and the rake face of the tool. Maximum strain is equal to 3.56 when rake angle is equal to -10º near the secondary shear zone. Maximum strain value reaches 2.85 when rake angle is equal to 0º and 10º.

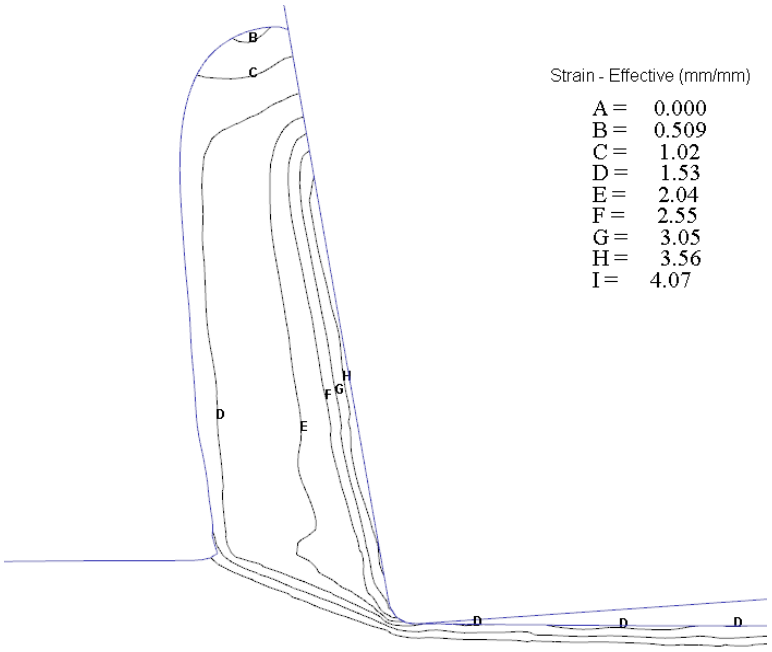

Figure 5.5. Strain distribution for α = -10º

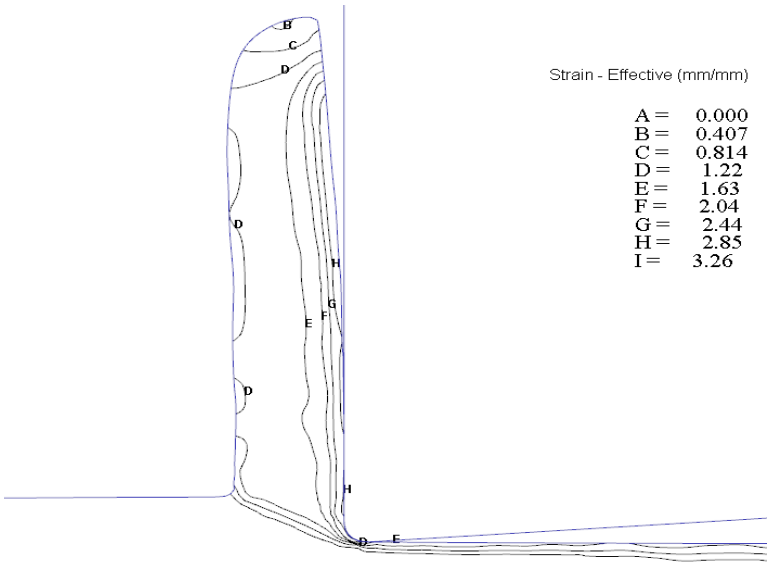

Figure 5.6. Strain distribution for α = 0º

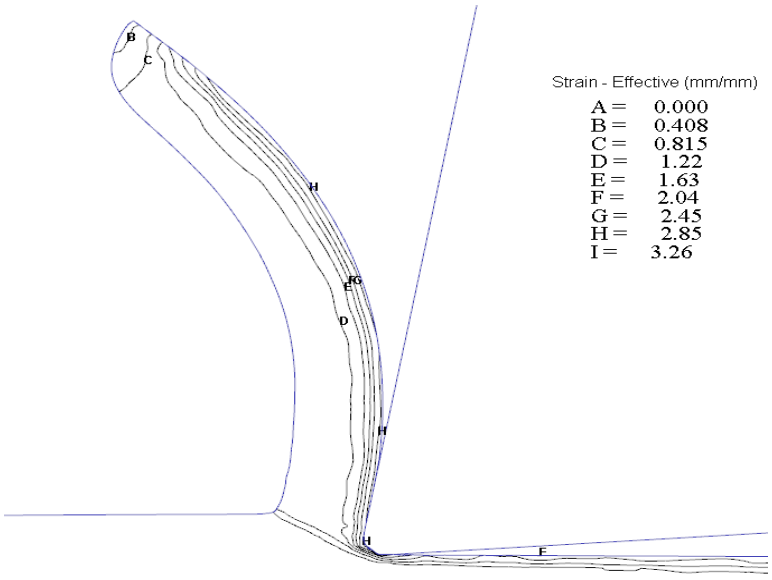

Figure 5.7. Strain distribution for α = 10º

Temperature contours are shown in Figure 5.8., Figure 5.9. and Figure 5.10. for different rake angles. Maximum cutting temperature is obtained when cutting with rake angle which is equal to -10º. The smallest cutting temperature which is equal to 439 ºC is obtained when rake angle is equal to 10º due to evolution of more curled chip and small contact length between the chip and the rake face. Although temperatures on the secondary shear zone are different than each other, temperatures on the primary shear zone are almost same.

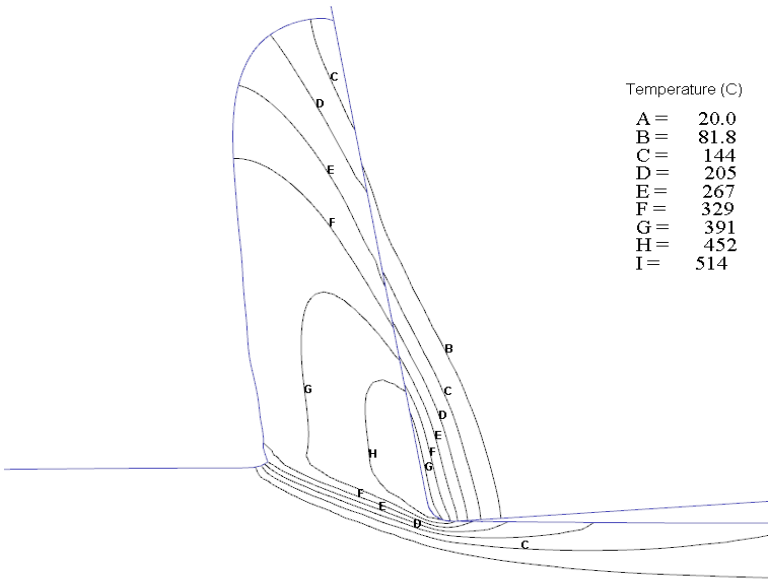

Figure 5.8. Temperature distribution for α = -10º

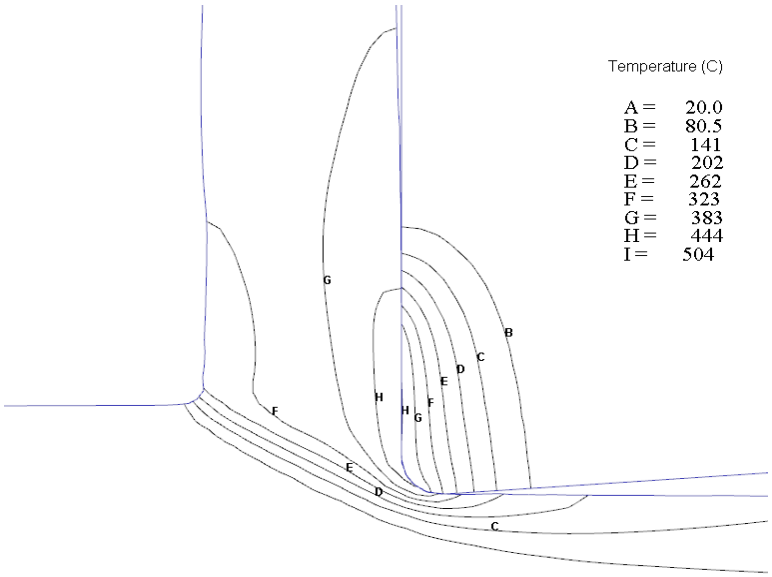

Figure 5.9. Temperature distribution for α = 0º

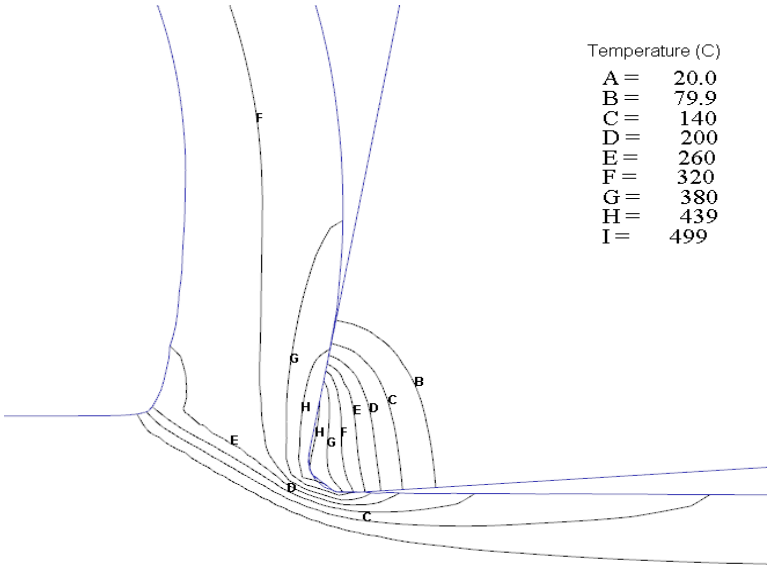

Figure 5.10. Temperature distribution for α = 10º

Effective stress distribution for different rake angles is shown in Figure 5.11., Figure 5.12. and Figure 5.13. Although maximum stress values do not considerably change, shape of stress field on the primary shear zone changes. When using -10º rake angle, stress field on the primary shear zone is narrower and a discontinuity is observed in front of the tool tip. In addition to this, a localised high stress value exists on the secondary shear zone. When rake angle becomes positive, stress field on the primary shear zone starts to extend toward flank surface of the tool.

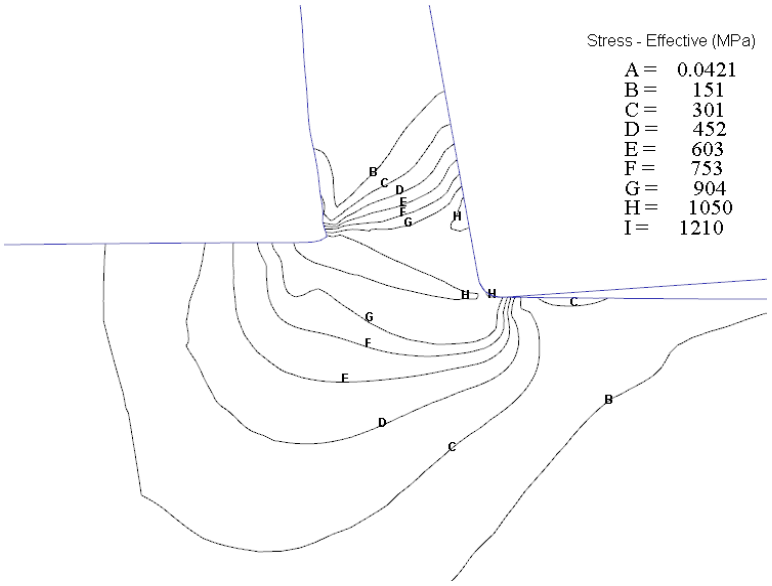

Figure 5.11. Effective stress distribution for α = -10º

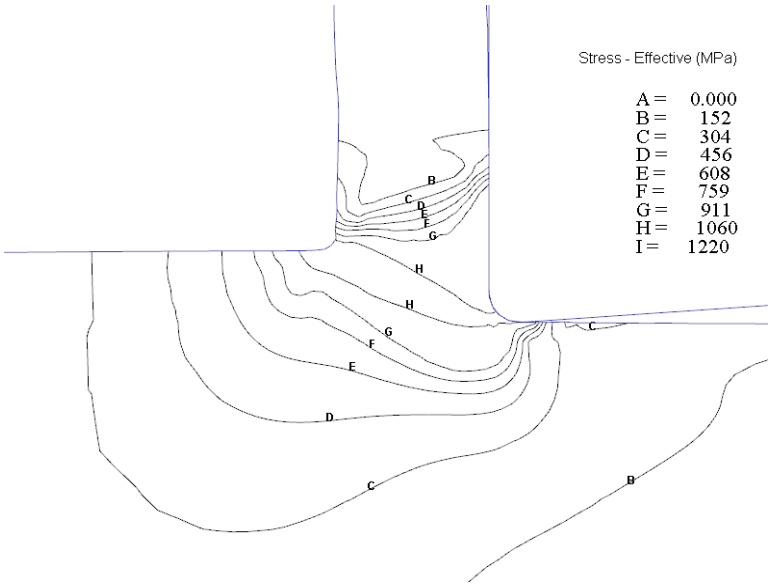

Figure 5.12. Effective stress distribution for α = 0º

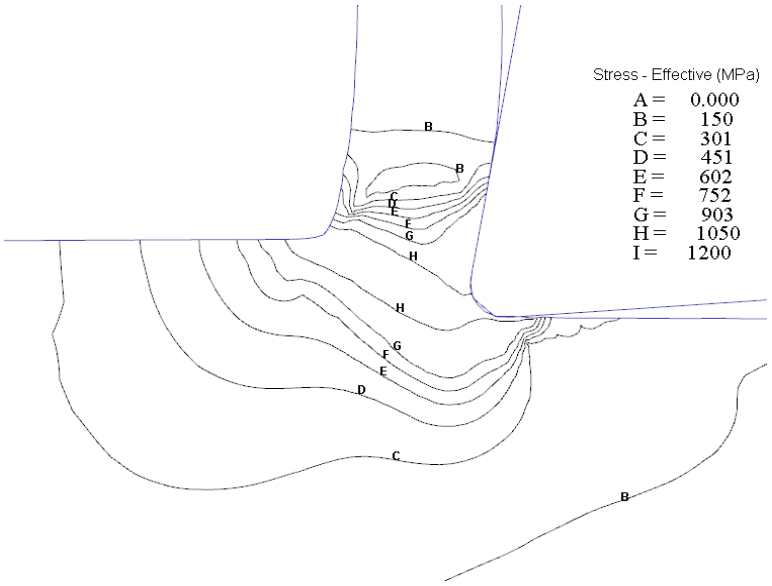

Figure 5.13. Effective stress distribution for α = 10º

To obtain steady state tool temperature and tool stress, additional calculation steps are performed after a Lagrangian analysis. Firstly, an Eulerian analysis is performed to obtain the steady state temperature in tool. After the steady state temperatures are obtained, one further Lagrangian analysis is carried out using an elastic tool to obtain tool stresses.

The steady state temperature distribution of tool for different rake angles is shown in Figure 5.14., Figure 5.15. and Figure 5.16. With the increase in the rake angle in negative way, more heat is generated due to increase in contact length between the chip and the rake angle and the amount of plastic formation. Maximum heat is located on the whole tool tip radius and some part of the rake face of the tool when rake angle is equal to 0º and 10º. However, when rake angle is equal to -10º, maximum heat occurs upon the tip radius of the tool.

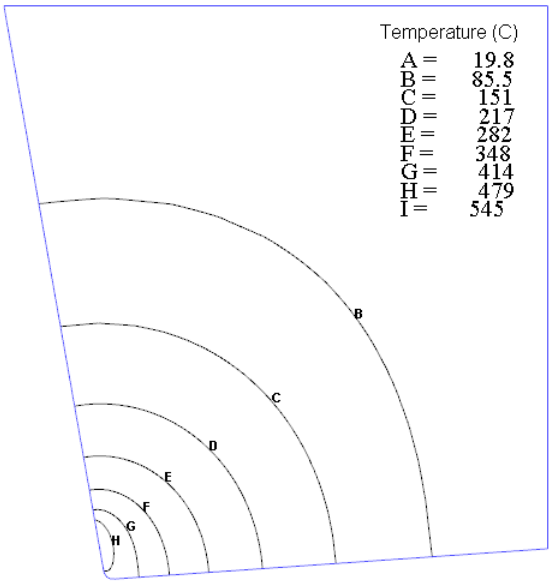

Figure 5.14. The steady state tool temperature for α = -10º

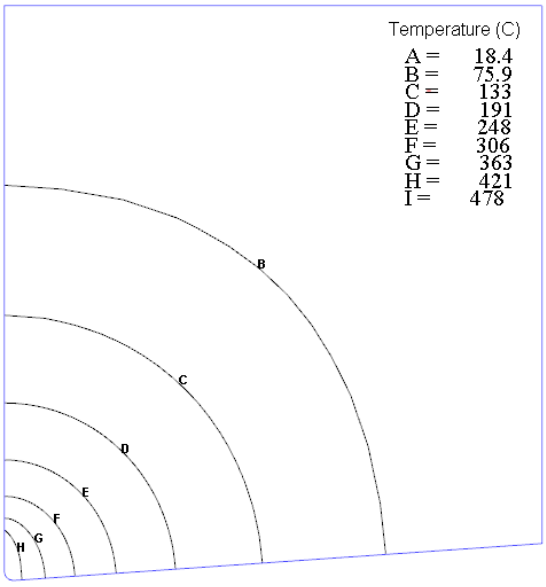

Figure 5.15. The steady state tool temperature for α = 0º

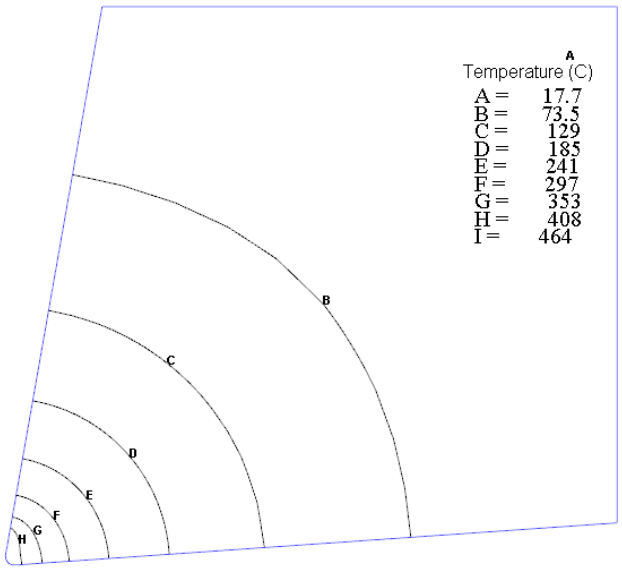

Figure 5.16. The steady state tool temperature for α = 10º

Tool stresses are shown in Figure 5.17., Figure 5.18. and Figure 5.19. It can be seen that the predicted tool stress increases with the negative rake angle usage. Maximum stress occurs on the flank surface of the tool near the tool tip radius for every rake angle. High stress (F contour) also occurs on the ahead of the tool tip. It is interesting to note that when rake angle is equal to 0º, stress on the tool tip and the flank surface is lower than other two.

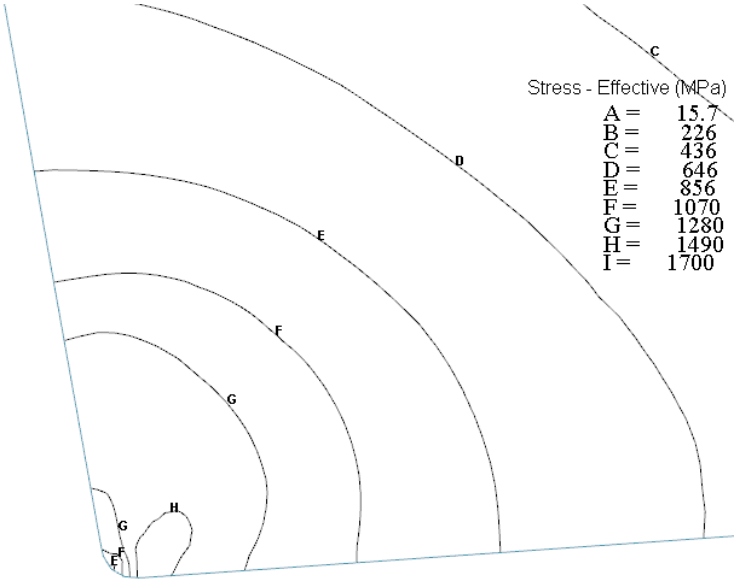

Figure 5.17. Stress distribution in the tool for α = -10º

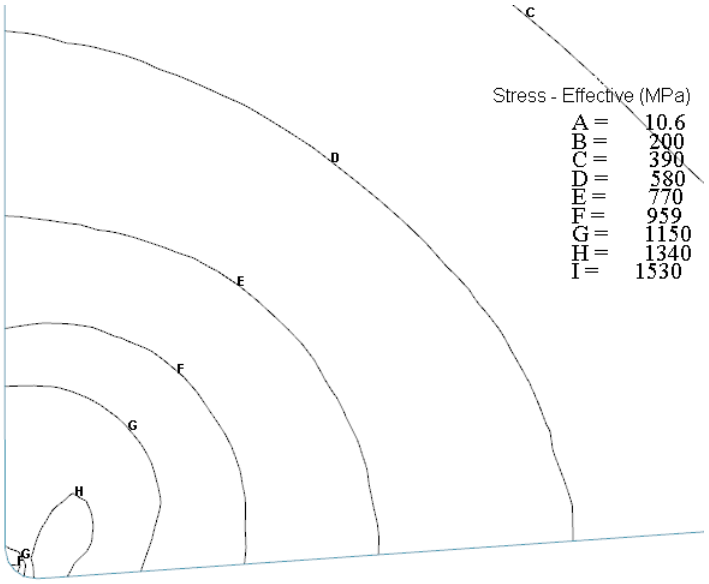

Figure 5.18. Stress distribution in the tool for α = 0º

Figure 5.19. Stress distribution in the tool for α = 10º

5.6. Effects of Tool Tip Radii

Effects of tool tip radii are investigated in this part of study by comparing strain distribution in work piece and steady state temperature and stress distribution of the tool. Three different tool tip radii (5 μm, 50 μm, 68 μm) are utilized and rake angle is fixed to 0º in the analysis.

Figure 5.20., Figure 5.21. and Figure 5.22. shows the predicted strain distributions in the work piece for different tool tip radii. It can be observed that plastic deformation in the secondary shear zone and on the machined surface increases when the tool tip radius increases.

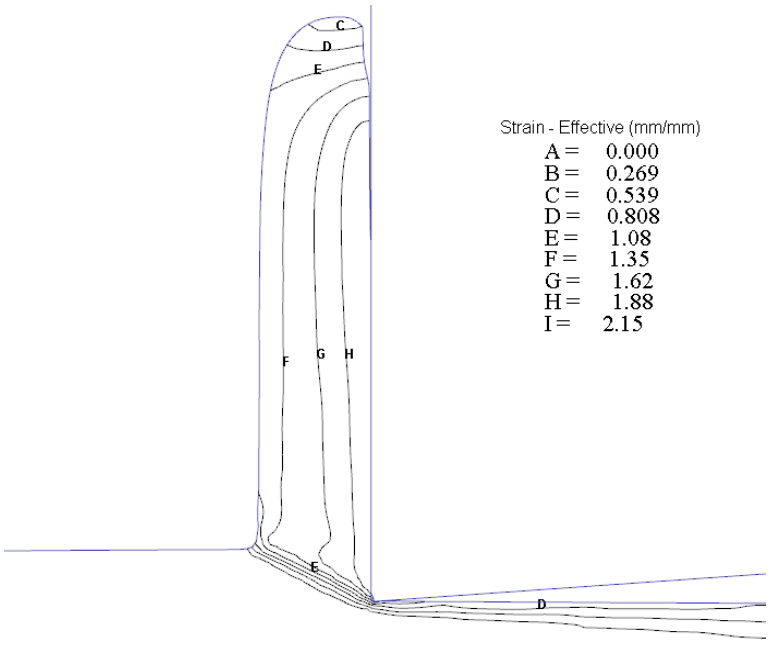

Figure 5.20. Strain distribution in the chip and the work piece for r_T = 5 µm

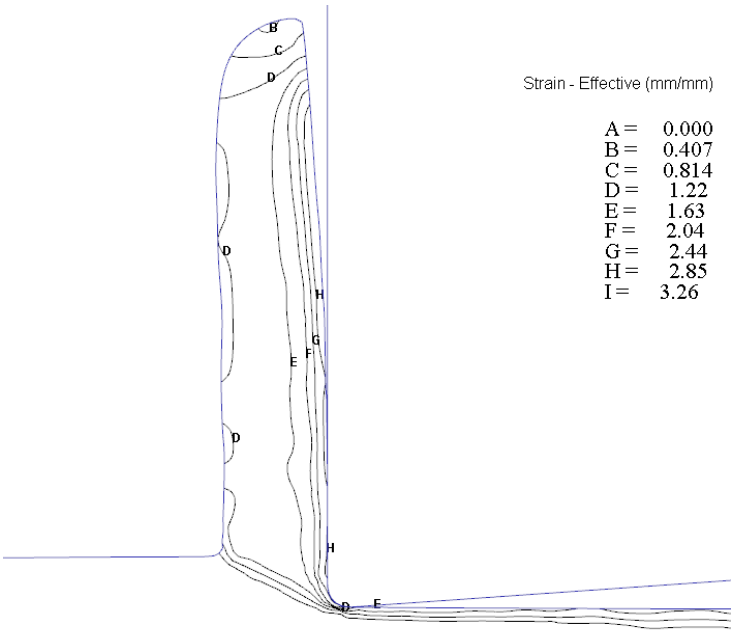

Figure 5.21. Strain distribution in the chip and the work piece for r_T = 50 µm

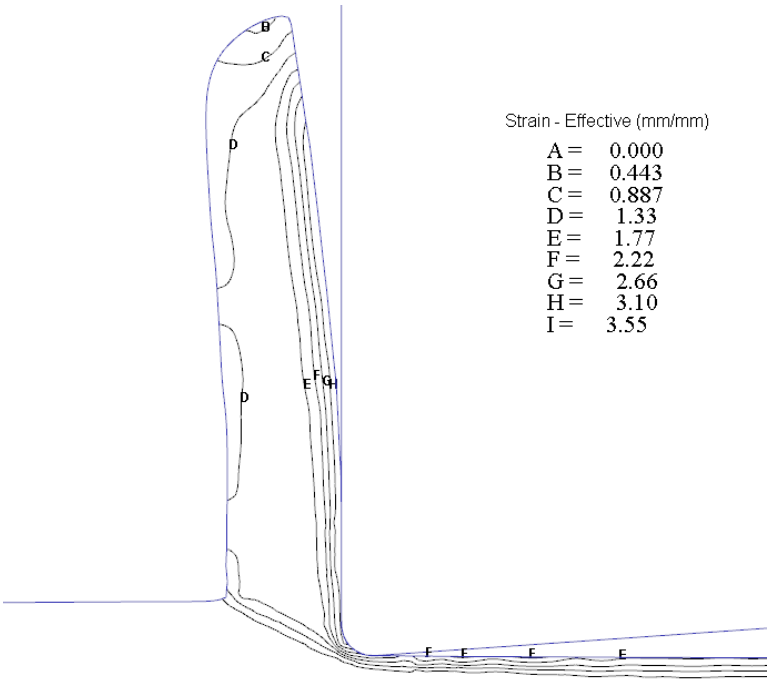

Figure 5.22. Strain distribution in the chip and the work piece for r_T = 68 µm

Figure 5.23., Figure 5.24. and Figure 5.25. shows the result of the steady state temperature distribution of the tool obtained for different tool tip radii. It can be seen that the increase of the tip radius leads to an increase in tool temperature. Main reason of that is the rubbing of the cutting edge on the machined surface. A minimum temperature occurs when tool tip radius is equal to 5 µm. For other tool tip radii, the maximum temperature in the tool becomes non sensitive to the size of the tip radius.

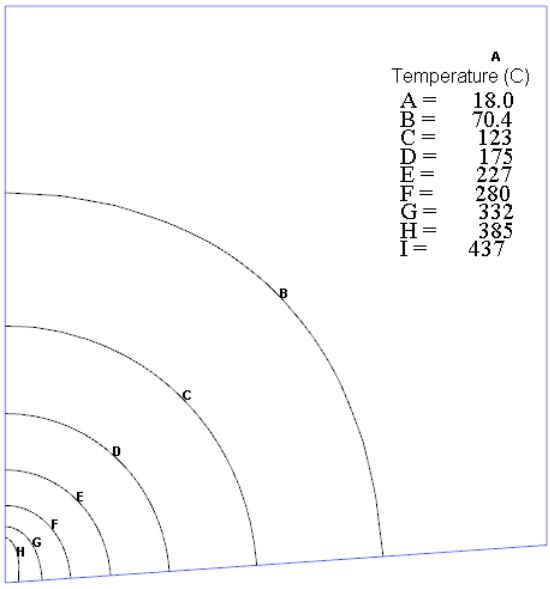

Figure 5.23. Temperature distribution in the tool for r_T = 5 µm

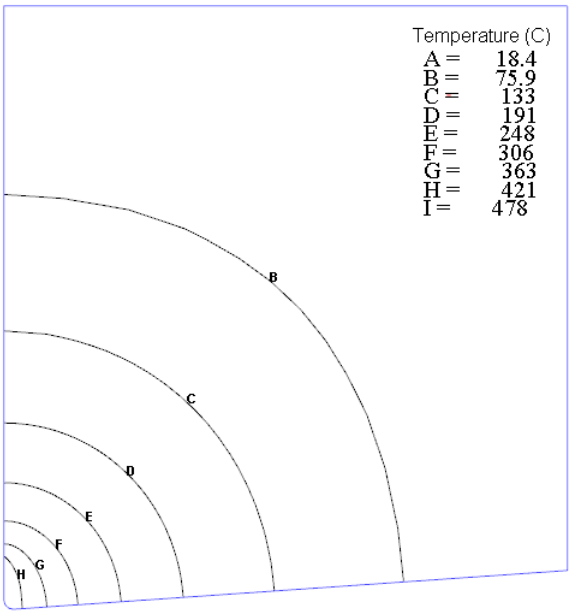

Figure 5.24. Temperature distribution in the tool for r_T = 50 µm

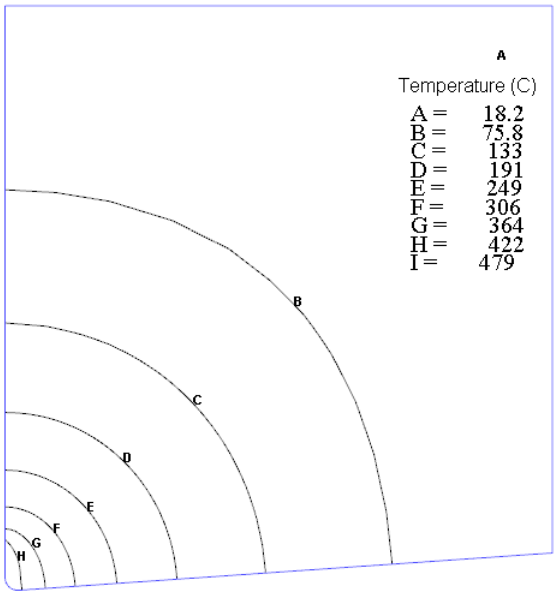

Figure 5.25. Temperature distribution in the tool for r_T = 68 µm

Predicted tool stress distribution for different tool tip radii is shown in Figure 5.26., Figure 5.27. and Figure 5.28. It is important to note that maximum stress in the tool is more concentrated near the tool tip (G profile) and the rake face of the tool (H profile) when tool tip radius is equal to 5 µm as shown in Figure 5.26. When tool tip radius increases, maximum tool stress tends to shift to the flank surface of the tool as shown in Figure 5.27. and Figure 5.28.

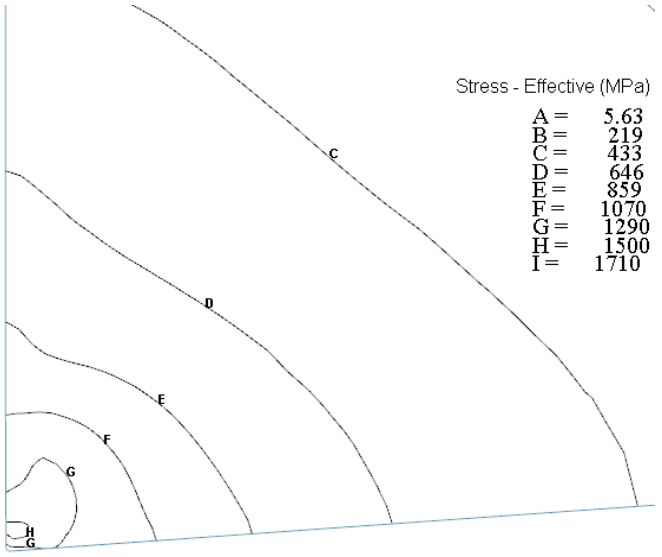

Figure 5.26. Stress distribution in the tool for r_T = 5 µm

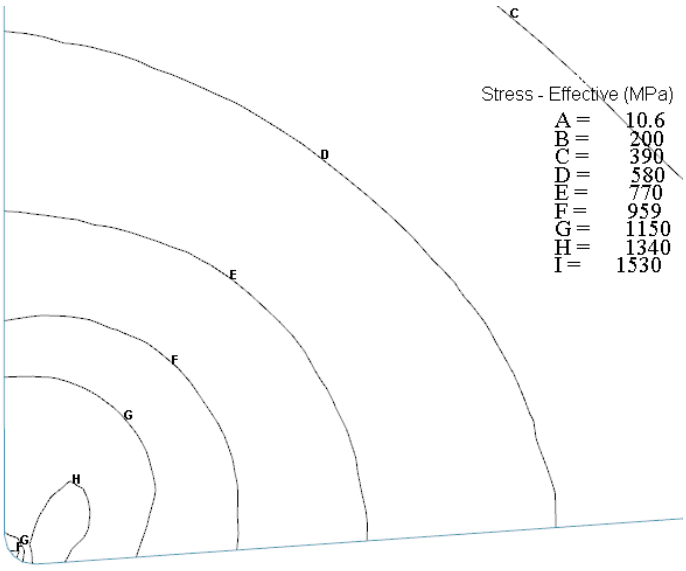

Figure 5.27. Stress distribution in the tool for r_T = 50 µm

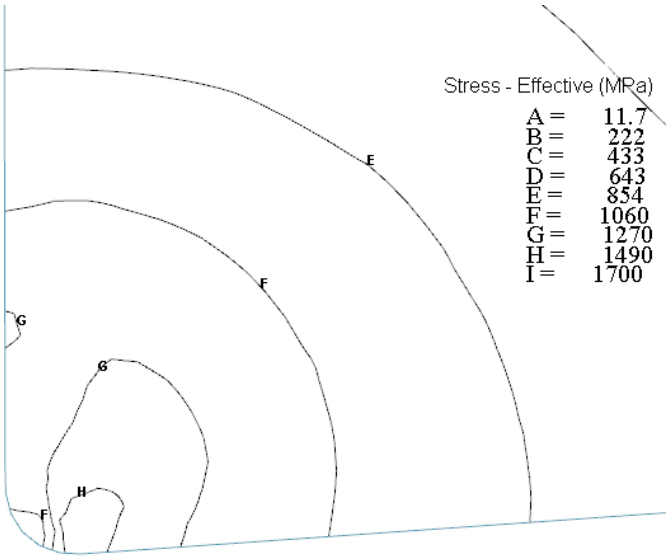

Figure 5.28. Stress distribution in the tool for r_T = 68 µm

CHAPTER 6

CONCLUSION

In this study, a thermo-mechanical model of plane strain orthogonal metal cutting with continuous chip formation is presented. The developed model is able to predict cutting and thrust forces, chip shape, chip thicknesses, contact lengths, shear angles as well as temperature, strain, strain rate and stress distributions.

In the first part of this study, three different material constitutive equations, two different friction models and one hybrid friction model are implemented, and results of model are compared with the experimental data available in the literature. It is seen that flow stress models have a major effect on calculated results. The results of the simulations show that Oxley material model is able to give more accurate results for used cutting conditions in the analysis, however errors in calculating shear angle and thrust force are higher than Johnson-Cook and Zerilli-Armstrong material models. In addition, friction models and friction coefficients have a strong influence on cutting forces, thrust forces, chip shape and temperature in the cutting zone. Followings are concluded for friction analysis;

1. Different friction coefficients must be tried to obtain more accurate results from the simulations. However, it is not a real case in a scientific view.
2. When friction coefficient is high, thrust force, chip thickness, contact length, shear angle and temperature are calculated quite well. Despite, error becomes high in calculated cutting force.
3. Coulomb friction model overestimates forces and temperature in contrast to Shear friction model when same friction coefficient is used. Therefore, small friction coefficients must be utilized for better results when Coulomb friction model is used. But it is not a realistic assumption.
4. It is seen that higher friction coefficient usage results in computational errors due to high element distortion in the analysis. Because of that, friction coefficients obtained from analytical relationships may not be used in finite element simulation of metal cutting.

In the following part of the study, it is seen that rake angle of the tool has a strong influence on plastic deformation in work piece, cutting temperature, contact length, steady state tool temperature and tool stress. The predictions show that the temperature on the tool increases when rake angle becomes negative which leads to more tool wear. However, this tendency is not observed for tool stress. When rake angle is equal to 0º, maximum stress on the tool is smaller than stress results of tools having -10º and 10º rake angles. Temperature increases with an increase in tool tip radius. It has been seen that when tip radius increases, maximum stress on the tool tends to move to flank surface which may cause flank wear. It is also observed that the maximum stresses are more concentrated in the tool tip which may cause plastic deformation of tool edge such as cracking when small tool tip radius is used. Lastly, more plastic deformation on the machined surface is generated when tip radius increases.

REFERENCES

Ambati, R. 2008. Simulation and Analysis of Orthogonal Cutting and Drilling Processes using LS-DYNA. *Msc. Thesis*. University of Stuttgart.

Armarego, E.J.A. and Brown, R.H. 1969. *The Machining of Metals*. New Jersey: Prentice-Hall.

Astakhov, V.P. 2006. *Tribology of Metal Cutting*. Oxford: Elsevier.

Astakhov, V.P. 2008. *Machining*. London: Springer.

Attanasio, A., Ceretti, E., Rizzuti, S., Umbrello, D. and Micari, F. 2008. 3D Finite Element Analysis of Tool Wear in Machining. *CIRP Annals Manufacturing Technology* 57: 61-64.

Bil, H., Kilic, S.E. and Tekkaya, A.E. 2004. A Comparison of Orthogonal Cutting Data from Experiments with Three Different Finite Element Models. *International Journal of Machine Tools and Manufacturing* 44: 933-944.

Boothroyd, G. 1981. *Fundamentals of Machining and Machine Tools*. Washington: Scripta Book Company.

Ceretti, E., Fallbohmer, P., Wu, W.T. and Altan, T. 1996. Application of 2D FEM to Chip Formation in Orthogonal Metal Cutting. *Journal of Materials and Processing Technology* 59: 169-180.

Chandrupatla, T.R. and Belegundu, A.D. 2002. *Introduction to Finite Element in Engineering*. New Jersey: Prentice-Hall.

Childs, T., Maekawa, K., Obikawa, T. and Yamane, Y. 2000. *Metal Machining Theory and Applications*. London: Arnold.

Clough, R.W. 1960. The Finite Element Method in Plane Stress Analysis. *Proceedings American Society of Civil Engineers* 23: 345-37.

Cocquilhat, M. 1851. Experiences Sur La Resistance Utile Produite Dans Le Forage. *Ann. Trav. Publ. En Belgique* 10: 199.

Cook, R.D., Malkus, D.S., and Plesha, M.E. 1989. *Concepts and Applications of Finite Element Analysis*. New York: John Wiley & Sons.

Courant, R. 1943. Variational Methods for the Solution of Problems of Equilibrium and Vibrations. *Bulletin of American Mathematical Society* 48: 1-23.

Davim, J.P. and Maranhao, C. 2009. A Study of Plastic Strain and Plastic Strain Rate in Machining of Steel AISI 1045 Using Fem Analysis. *Materials and Design* 30: 160-165.

DeGarmo, E.P., Black, J.T. and Kosher, R.A. 1997. *Materials and Processes in Manufacturing* New Jersey: Prentice-Hall.

Dogu, Y., Aslan, E. and Camuscu N. 2006. A Numerical Model to Determine Temperature Distribution in Orthogonal Metal Cutting. *Journal of Materials and Processing Technology* 171: 1-9.

Ernest, H. and Merchant, M.E. 1941. Chip Formation, Friction and High Quality Machined Surfaces. *Transactions of American Society for Metals* 29: 299-378.

Filice, L., Micari, F., Rizutti, S. and Umbrello, D. 2007. A Critical Analysis On the Friction Modelling in Orthogonal Machining. *International Journal of Machine Tools and Manufacturing* 47: 709-714.

Grzesik, W. 2008. *Advanced Machining Processes of Metallic Materials*. Oxford: Elsevier.

Jaspers, S.P.F.C. and Dautzenberg, J.H. 2002. Material Behaviour in Conditions Similar to Metal Cutting; Flow Stress in the Shear Zone. *Journal of Materials and Processing Technology* 122: 322-330.

Johnson, G.R. and Cook, W.H. 1993. A Constitutive Model and Data for Metals Subjected to Large Strains, High Strain-rates and High Temperatures. *Seventh International Symposium on Ballistics* 7: 541-547.

Kapakjian, S. and Schmid, S.R. 2006. *Manufactruing Engineering and Technologhy*. New Jersey: Prentice-Hall.

Kim, K.W., Lee, W.Y. and Sin, H. 1999. A Finite Element Analysis for the Chracteristics of Temperature and Stress in Micro-machining Considering the Size Effect. *International Journal of Machine Tools and Manufacturing* 39: 1507-1524.

Klamecki, B.E. 1973. Incipient Chip Formation in Metal Cutting- A Three Dimension Finite Element Analysis. *PhD. Thesis*. University of Illinois at Urbana-Champain.

Kobayashi, S. and Thomsen, E.G. 1962. Metal Cutting Analysis II New Parameters. *Journal of Engineering for Industry* 84: 71-80.

Komvopoulos, K. and Erpenbeck, S.A. 1991. Finite Element Modeling of Orthogonal Metal Cutting. *Trans. ASME J. Eng. Ind*. 113: 253-267.

Lee, E.H and Shaffer, B.W. 1951. The Theory of Plasticity Applied to a Problem of Machining. *Journal of Applied Mechanics* 18: 405-413.

Lin, Z.C. and Lin, S.Y. 1992. A Coupled Finite Element Model of Thermo-Elastic-Plastic Large Deformation for Orthogonal Cutting. *Journal of Engineering Materials Technology* 114(2): 31-48.

Maekawa, K., Nagayama, T., Okushima, I. and Murata, R. 1990. Finite Element Simulation of Oblique Cutting. *Bulletin of Jpn. Soc. Precis. Eng*. 24(3): 221-222.

Mamalis, A.G., Horvath, M., Branis, A.S. and Manolakos, D.E. 2001. Finite Element Simulation of Chip Formation in Orthogonal Metal Cutting. *Journal of Materials and Processing Technology* 110: 19-27.

Merchant, M.E. 1945. Mechanics of Metal Cutting Process. *Journal of Applied Physics* 16: 267-318.

Mohr, G.A. (1992). *Finite Element for Solids, Fluids and Optimization*. Oxford: Oxford University Press.

Okushima, K. and Hitomi, K. 1961. An Analysis of the Mechanics of Orthogonal Cutting and Its Application to Discontinuous Chip Formation. *Trans. Amer. Soc. Mech. Engrs*. Series B J. of Eng. 83: 545.

Oxley, P.L.B. 1961. A Strain Hardening Solution for the Shear Angle in Orthogonal Metal Cutting. *International Journal of Mechanics Science* 3: 68.

Oxley, P.L.B. 1990. Mechanics of Machining: An Analytical Approach to Assessing Machinability. *Journal of Applied Mechanics* 57: 253.

Oxley, P.L.B. and Welsh, M.J.M. 1963. Calculating the Shear Angle in Orthogonal Metal Cutting from Fundamental Stress, Strain, Strain-rate Properties of the Work piece Material. *Proceedings of the Fourth International Conference on Machine Tool Design and Research Conference* 4: 73-86.

Ozel, T. 2006. The Influence of Friction Models On Finite Element Simulations of Machining. *International Journal of Tools and Manufacturing* 46: 518-530.

Ozel, T. and Zeren, E. 2007. Finite Element Modelling the Influence of Edge Roundness on the Stress and Temperature Fields Induced by High Speed Machining. *International Journal of Advanced Manufacturing Technology* 35: 255-267.

Palmer, W.B. and Oxley, P.L.B. 1959. Mechanics of Orthogonal Machining. *Proc. Inst. Mech. Engrs*. 173: 623.

Petrarius, V., Amorande, D. and Alaci, S. 2008. Study about Finite Element Analysis of High Speed Drilling. *Fascile of Management and Technological Engineering* 11.

Shatla, M., Kerk, C. and Altan, T. 2001. Process Modelling in Machining. Part II: Validation and Applications of the Determined Flow Stress Data. *International Journal of Tools and Manufacturing* 41: 1659-1680.

Shaw, M.C. 1989. *Metal Cutting Principles*. New York: Oxford University Press.

Strenkowski, J.S. and Carroll, J.T. 1985. A Finite Element Model of Orthogonal Metal Cutting. *Trans. ASME J.Eng. Ind*. 107: 349-354.

Tresca, H. 1878. On Further Applications of the Flow Solids. *Proc. I. Mech. E. Lond*. 1: 301-345.

Ushi, E. and Shirakashi, T. 1982. Mechanics of Machining from Descriptive to Predictive Theory. *On the Art of Cutting Metals- 75 Years Later* 7: 13-55.

Vaz, M., Owen, D.R.J., Kalhori, V., Lundblad, M. and Lindgren, L.E. 2007. Modelling and Simulation of Machining Processes. *Arc. Comput. Methods Eng*. 14: 173-204.

Zerilli, F.J. and Armstrong, R.W. 1987. Dislocation Mechanics Based Constitutive Relations for Materials Dynamics Calculations. *Journal of Applied Physics* 5: 61.

Zienkiewicz, O.C. and Cheung, Y.K. 1967. *The Finite Element Method in Structural and Continuum Mechanics*. London: Mc-Graw Hill.

Zorev, N.N. 1963. Inter-relationship between Shear Processes Occurring along the Tool Face and Shear Plane in Metal Cutting. *International Research in Production Enginerring ASME* 42-49.